

# HOMOGENIZATION OF THE STEFAN PROBLEM, WITH APPLICATION TO MAPLE SAP EXUDATION\*

ISABELL GRAF<sup>†‡</sup> AND JOHN M. STOCKIE<sup>‡</sup>

**Abstract.** The technique of periodic homogenization with two-scale convergence is applied to the analysis of a two-phase Stefan-type problem that arises in the study of a periodic array of melting ice bars. For this “reduced model” we prove results on existence, uniqueness and convergence of the two-scale limit solution in the weak form, which requires solving a macroscale problem for the global temperature field and a reference cell problem at each point in space which captures the underlying phase change process occurring on the microscale. We state a corresponding strong formulation of the limit problem and use it to design an efficient numerical solution algorithm. The same homogenized temperature equations are then applied to solve a much more complicated problem involving multi-phase flow and heat transport in trees, where the sap is present in both frozen and liquid forms and a third gas phase is also present. Our homogenization approach has the advantage that the global temperature field is a solution of the same reduced model equations, while all the remaining physics are relegated to the reference cell problem. Numerical simulations are performed to validate our results and draw conclusions regarding the phenomenon known as sap exudation, which is of great importance in sugar maple trees and few other related species.

**Key words.** periodic homogenization, two-scale convergence, Stefan problem, multiphase flow, phase change, sap exudation

**AMS subject classifications.** 35B27, 35R37, 76T30, 80A22, 92C80

**1. Introduction.** Multiscale problems are characterized by geometric, material or other features that exhibit variations on spatial or temporal scales that differ widely. Many mathematical and numerical methods have been derived for dealing with this scale separation and accurately capturing the interactions between phenomena operating on different scales. For problems that have a periodic microstructure, one such mathematical approach is periodic homogenization, and more specifically the approach known as two-scale asymptotic convergence [1].

In this paper, we are interested in applying two-scale convergence to analyze solutions of a Stefan-type problem that arises from multi-phase flow in a porous medium coupled with heat transport. In particular, we are motivated by the study of sap flow in a maple tree that is subject to both thawing and freezing [5]. We seek insight into the phenomenon called *sap exudation*, which refers to the generation of elevated sap pressure within the maple tree trunk in advance of the spring thaw when the tree is still in a leafless state and no photosynthesis (or transpiration) occurs to drive the sap flow. Our work is based on the model derived in [5] that captures the physical processes going on at the microscale (that is, at the level of individual wood cells) and includes multiphase flow of gas/ice/water, heat transport, porous flow through cell walls, and osmotic effects. There is an inherent repeating structure in wood at the cellular scale that lends itself naturally to a homogenization approach, although with the exception of the analysis of [6] for water transport in plant tissues, the application of homogenization techniques in the context of heat or sap flow in trees is very limited.

Before tackling the sap exudation problem in its full complexity, it is convenient to first develop our homogenization approach in the context of a simpler “reduced model” that focuses only on heat transport and ice/water phase change for a similarly fine-structured domain. To this end, we consider in Section 2 the transport of heat in a region containing a periodic array of small cylindrical ice bars immersed in water. The temperature field obeys the heat equation, and is coupled with a Stefan condition at the ice/water phase interface that governs the transition from solid to liquid and vice versa. Many different approaches have been developed to analyze such phase transitions, and these are well-described in the monograph [24]. To handle the multiplicity of the ice bars, we apply the technique of periodic homogenization with two-scale convergence established in [1, 21]. Several authors have previously applied homogenization to solving the Stefan problem, such as in [3, 8, 25] where the phase change boundary is handled by separately homogenizing an auxiliary problem. In [9] on the other hand, an additional function  $\theta$  is introduced for an aggregate state that diffuses on a slow time scale and with which all microscopic phase changes are properly captured.

---

Latest revision: November 25, 2021.

\*This work was supported in part by a Discovery Grant from the Natural Sciences and Engineering Research Council of Canada.

<sup>†</sup>Corresponding author. IG was supported by a Feodor Lynen Fellowship from the Alexander von Humboldt Foundation.

<sup>‡</sup>Department of Mathematics, Simon Fraser University, 8888 University Drive, Burnaby, BC, V5A 1S6, Canada (grafisab@gmail.com, stockie@math.sfu.ca).

The approach we employ in this paper has the advantage that it applies homogenization techniques in a straightforward manner in order to obtain an uncomplicated limit model, the simplicity of which ensures that numerical simulations are relatively easy to perform. More specifically, we define a reference cell  $Y$  that is divided into two sub-regions:  $Y^1$  where the temperature diffuses rapidly; and  $Y^2$  where we define a second temperature field that diffuses slowly. One particular challenge that arises in the study of Stefan problems is that the diffusion coefficient depends on the underlying phases, so that heat diffuses differently in water or ice. Consequently, the diffusion coefficient depends on temperature (or equivalently on enthalpy) so that the governing differential equation is only quasi-linear.

The details of our periodic homogenization approach are introduced in the context of the reduced model in Section 2.1. We prove the existence of a solution of the governing PDE in Section 2.2 and derive a priori estimates of the solution in Section 2.3. The identification of the two-scale limit equations is performed in Section 2.4, and uniqueness of the limit problem is proven in Section 2.5. Finally, we provide the strong formulation and one-phase formulation of the limit problem in Section 2.6. Detailed proofs of the lemmas and theorems involved are relegated to the Appendices. We conclude our study of the reduced model in Section 3 with numerical simulations that illustrate the behaviour of the homogenized solution.

The remainder of the paper focuses on the application of our periodic homogenization approach to the maple sap exudation problem. We aim to extend the homogenized equation derived earlier for the reduced model to obtain a corresponding homogenized equation that governs freezing/thawing in maple sap, and this process is carefully justified in the introduction to Section 4. The governing equations for the sap exudation problem on the cellular scale are a slightly modified version of the model developed in [5] which we summarize in Section 4.2. The major advantage of our approach is that the homogenized equations for the two-phase reduced problem can also be used to determine the temperature in the more complicated sap exudation problem, with the added complexity of the extra gas phase, dynamic phase interfaces, pressure exchange, etc. all confined to the reference cell. Guided by our experience with the reduced model, we develop a corresponding numerical algorithm for solving the homogenized sap exudation model, and then present simulations in Section 4.3 that we compare with results from the reduced model. Finally, we conclude in Section 5 with a discussion of the biological significance of our results in the context of tree sap flow, and we suggest several exciting avenues for future work that exploit our homogenized sap exudation model.

## 2. Reduced model: Ice bars melting in water.

**2.1. Mathematical formulation.** Let  $\Omega \subset \mathbb{R}^n$  be a bounded domain having Lipschitz boundary and that contains both water and ice, where the ice takes the form of “bars” occurring in a regular repeating pattern such as that shown in Figure 1(a). Let  $Y = [0, \delta]^n$  be a *reference cell* that captures the configuration of the periodic microstructure, and for which  $\delta$  represents its physical size and  $0 \leq \delta \ll 1$ . The reference cell is divided into two sub-domains  $Y^1$  and  $Y^2$  that are separated by a Lipschitz boundary  $\Gamma = Y^1 \cap Y^2$ . The primary feature that we exploit in our homogenization approach is that within  $Y^1$  heat diffuses rapidly, whereas in  $Y^2$  there is instead a relatively slow diffusion of heat. We take  $\Gamma$  to be a circle of radius  $\gamma$  that satisfies  $0 < \gamma < \delta$ . A picture illustrating this decomposition of the reference cell is given in Figure 1(b).

We next introduce a small parameter  $0 < \varepsilon \ll 1$  that corresponds to the size of the periodic microstructure. The domain  $\Omega$  may then be decomposed into three  $\varepsilon$ -dependent sub-domains:  $\Omega_\varepsilon^1 := \bigcup_{k \in \mathbb{Z}^n} \varepsilon(k + Y^1) \cap \Omega$  (which is connected), and two disconnected components consisting of the region  $\Omega_\varepsilon^2 := \bigcup_{k \in \mathbb{Z}^n} \varepsilon(k + Y^2) \cap \Omega$  and the boundary curves  $\Gamma_\varepsilon := \bigcup_{k \in \mathbb{Z}^n} \varepsilon(k + \Gamma) \cap \Omega$ . This decomposition is highlighted in Figure 1(a).

Throughout the theoretical derivations in this paper, we employ what is known as the two-phase formulation of the Stefan problem in which the heat diffusion equation does not involve the time rate of change of temperature but rather that of the specific enthalpy  $E$ , which measures the heat energy stored in the water or ice per unit mass and has units of  $J/kg$ . Assuming that the material properties for water and ice remain constant in their respective phase, the temperature  $T$  (in  $^\circ K$ ) can be written as a piecewise linear function

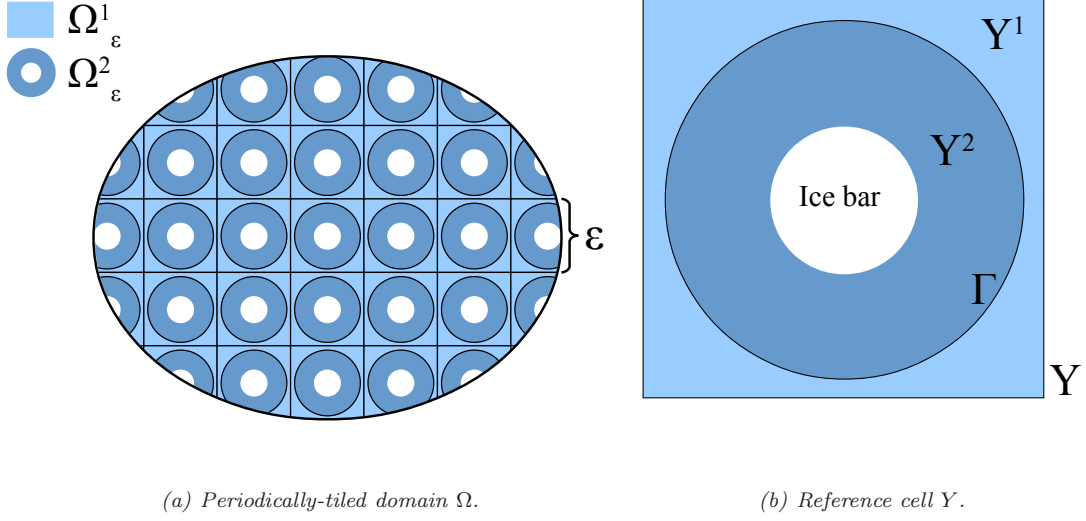


FIGURE 1. Periodic microstructure of the reduced model with ice bars immersed in water, illustrating the decomposition into fast ( $Y^1$  and  $\Omega_\varepsilon^1$ ) and slow ( $Y^2$  and  $\Omega_\varepsilon^2$ ) diffusing regions.

of enthalpy [24]

$$T = \tilde{\omega}(E) = \begin{cases} \frac{1}{c_i}E, & \text{if } E < E_i, \\ T_c, & \text{if } E_i \leq E < E_w, \\ T_c + \frac{1}{c_w}(E - E_w), & \text{if } E_w \leq E, \end{cases}$$

where  $T_c = 273.15^\circ K$  is the melting/freezing point of water,  $c$  denotes specific heat ( $J/kg^\circ K$ ), and  $E$  denotes the enthalpy ( $J/kg$ ) at  $T = T_c$ . The subscripts  $i$  and  $w$  refer to the ice and water phases, respectively. A distinguishing feature of this temperature-enthalpy relationship is that when the temperature is equal to the melting point, the enthalpy varies while the temperature remains constant – this behavior derives from the fact that a certain amount of energy (known as latent heat) is required to effect a change in phase from solid to liquid at the interface between phases.

Because the function  $\tilde{\omega}(E)$  above is neither differentiable nor invertible, we instead employ in our model a regularized function  $\omega(E)$  with “rounded corners” such as that pictured in Figure 2, which is incidentally a better representation of what one would actually observe in a real physical system:

$$(2.1) \quad T = \omega(E) = \begin{cases} \frac{1}{c_i}E, & \text{if } E < E_i^1, \\ \text{[smooth connection]}, & \text{if } E_i^1 \leq E < E_i^2, \\ T_c - \frac{2E - (E_i^2 + E_w^1)}{2c_\infty}, & \text{if } E_i^2 \leq E < E_w^1, \\ \text{[smooth connection]}, & \text{if } E_w^1 \leq E < E_w^2, \\ T_c + \frac{1}{c_w}(E - E_w^2), & \text{if } E_w^2 \leq E. \end{cases}$$

The nearly flat portion of the temperature curve in the transition region near  $T \approx T_c$  has a small positive slope  $\frac{1}{c_\infty}$ , and the corners are smoothed out over the short intervals  $E_i^1 \lesssim E_i \lesssim E_i^2$  and  $E_w^1 \lesssim E_w \lesssim E_w^2$ . These smooth connections ensure that  $\omega$  is a continuously differentiable, invertible and monotone increasing function of enthalpy.

We now describe the decomposition of the solution into slow and fast diffusing variables. The functions  $T_{1,\varepsilon}$  and  $E_{1,\varepsilon}$  denote the fast-diffusing temperature and enthalpy components (respectively) and are defined

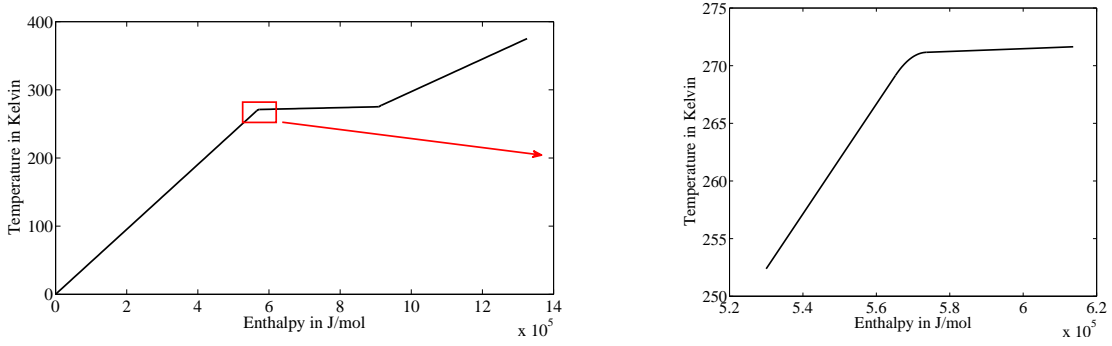


FIGURE 2. Plot of the temperature-enthalpy function,  $T = \omega(E)$ , for a generic ice/water phase change problem in which the critical (melting) temperature is  $T_c = 273.15^\circ K$ . The zoomed-in view on the right illustrates the smoothed corners in the regularization.

on the sub-region  $\Omega_\varepsilon^1$ . Similarly,  $T_{2,\varepsilon}$  and  $E_{2,\varepsilon}$  are the slow-diffusing temperature and enthalpy defined on  $\Omega_\varepsilon^2$ . Next, we define the corresponding solution spaces

$$\begin{aligned}\mathcal{V}_\varepsilon^1 &:= \{u \in L^2([0, t_m], \mathcal{H}^1(\Omega_\varepsilon^1)) \cap \mathcal{H}^1([0, t_m], \mathcal{H}^1(\Omega_\varepsilon^1)') \mid u = 0 \text{ on } \partial\Omega_\varepsilon^1 \cap \partial\Omega\}, \\ \mathcal{V}_\varepsilon^2 &:= \{u \in L^2([0, t_m], \mathcal{H}^1(\Omega_\varepsilon^2)) \cap \mathcal{H}^1([0, t_m], \mathcal{H}^1(\Omega_\varepsilon^2)') \mid u = 0 \text{ on } \Gamma_\varepsilon\},\end{aligned}$$

where the “prime” is used to denote a dual space and  $[0, t_m]$  represents the time interval of interest for some fixed  $t_m > 0$ . The corresponding test spaces are  $V_\varepsilon^1 = \mathcal{H}^1(\Omega_\varepsilon^1)$  and  $V_\varepsilon^2 = \mathcal{H}_0^1(\Omega_\varepsilon^2)$ . We also need to introduce notation for inner products, with  $(u, v)_{\Omega_\varepsilon^\alpha} = \int_{\Omega_\varepsilon^\alpha} uv \, dx$  representing the inner product of two functions in  $\mathcal{V}_\varepsilon^\alpha$  for  $\alpha = 1, 2$ , whereas  $(u, v)_{\Omega_\varepsilon^\alpha, t} = \int_0^t \int_{\Omega_\varepsilon^\alpha} uv \, dx \, d\tau$  denotes that an additional time integration is performed over the interval  $[0, t]$  with  $0 \leq t \leq t_m$ . Finally, we let  $\langle u, v \rangle_{\Gamma_\varepsilon} = \int_{\Gamma_\varepsilon} g_\varepsilon uv \, d\sigma_x$  denote the inner product on the interface  $\Gamma_\varepsilon$ , where  $g_\varepsilon$  represents the Riemann curvature tensor.

We are now prepared to state the weak form of the heat diffusion problem. Assuming that initial values  $T_{1,\varepsilon,init} = \omega(E_{1,\varepsilon,init})$  and  $T_{2,\varepsilon,init} = \omega(E_{2,\varepsilon,init})$  are smooth, non-negative and bounded, and that a Dirichlet condition  $T_{1,\varepsilon} = T_a$  is imposed at the outer boundary  $\partial\Omega \cap \partial\Omega_\varepsilon^1$ , our goal is to find  $(T_{1,\varepsilon}, T_{2,\varepsilon}) \in (\mathcal{V}^1 + T_a) \times (\mathcal{V}^2 + T_{1,\varepsilon})$  such that

$$(2.2a) \quad (\partial_t E_{1,\varepsilon}, \varphi)_{\Omega_\varepsilon^1} + (D(E_{1,\varepsilon}) \nabla T_{1,\varepsilon}, \nabla \varphi)_{\Omega_\varepsilon^1} + \varepsilon^2 \langle D(E_{2,\varepsilon}) \nabla T_{2,\varepsilon} \cdot \mathbf{n}, \varphi \rangle_{\Gamma_\varepsilon} = 0,$$

$$(2.2b) \quad (\partial_t E_{2,\varepsilon}, \psi)_{\Omega_\varepsilon^2} + (\varepsilon^2 D(E_{2,\varepsilon}) \nabla T_{2,\varepsilon}, \nabla \psi)_{\Omega_\varepsilon^2} = 0,$$

for all  $\varphi, \psi \in V^1 \times V^2$ . Note that  $\mathbf{n}$  represents the outward-pointing unit normal vector on  $\Omega_\varepsilon^2$ , and that the temperature and enthalpy are connected via  $T_{\alpha,\varepsilon} = \omega(E_{\alpha,\varepsilon})$ , or equivalently  $E_{\alpha,\varepsilon} = \omega^{-1}(T_{\alpha,\varepsilon})$ . Following [24], we take the diffusion coefficient to be a piecewise affine linear function of enthalpy

$$(2.3) \quad D(E) = \begin{cases} \frac{k_i}{\rho_i}, & \text{if } E < E_i, \\ \frac{k_i}{\rho_i} + \frac{E - E_i}{E_w - E_i} \left( \frac{k_w}{\rho_w} - \frac{k_i}{\rho_i} \right), & \text{if } E_i \leq E < E_w, \\ \frac{k_w}{\rho_w}, & \text{if } E_w < E, \end{cases}$$

where  $\rho_w$  and  $\rho_i$  are water and ice densities ( $kg/m^3$ ),  $k_w$  and  $k_i$  are thermal conductivities ( $W/m^\circ K$ ), and  $E_w$  and  $E_i$  are the corresponding enthalpies at  $T = T_c$ . We note in closing that slow diffusion is induced in our problem by the factor  $\varepsilon^2$  multiplying terms in Eqs. (2.2) that involve the diffusion coefficient  $D(E_{2,\varepsilon})$ .

The following four sections contain the primary theoretical results relating to solutions of the reduced problem in the weak form.

**2.2. Existence.** To prove the existence of a solution to (2.2) for every  $\varepsilon > 0$ , we employ a result of Showalter [22, Prop. 4.1 ( $p = 2$ )]. Let  $V$  represent a reflexive Banach space with dual  $V'$  and let  $\mathcal{V} = L^2([0, t_m], V)$  with dual  $\mathcal{V}' = L^2([0, t_m], V')$ . We also have the Hilbert space  $H$  with  $V \subset H \subset V'$ , where  $V$  is dense and continuously embedded in  $H$ .

**2.2.1. General function space setting.** Suppose that  $\mathcal{A} : V \rightarrow V'$  is a given function (not necessarily linear) where  $u_0 \in H$  and  $f \in \mathcal{V}'$ . We are interested in finding  $u \in \mathcal{V}$  such that

$$(2.4) \quad \int_0^{t_m} \partial_t u(t) v(t) dt + \int_0^{t_m} \mathcal{A}(u(t)) v(t) dt = \int_0^{t_m} f(t) v(t) dt,$$

with  $u(0) = u_0 \in H$  for every  $v \in \mathcal{V}$ . That is,  $\mathcal{V}$  is the solution and the test space.

**DEFINITION 2.1.** *An operator  $\mathcal{A}$  is hemicontinuous if for each  $u, v \in V$ , the real-valued function  $\beta \mapsto \mathcal{A}(u + \beta v)v$  is continuous.*

**SHOWALTER'S PROPOSITION (PROP. 4.1 IN [22])** *Let the spaces  $V, H, \mathcal{V}$  be defined as above and assume that  $V$  is separable. Consider the family of operators  $\mathcal{A}(t, \cdot) : V \rightarrow V'$  for  $0 \leq t \leq t_m$  that satisfy the following conditions:*

- (i) *for each  $v \in V$  the function  $\mathcal{A}(\cdot, v) : [0, t_m] \rightarrow V'$  is measurable;*
- (ii) *for almost every  $t \in [0, t_m]$  the operator  $\mathcal{A}(t, \cdot) : V \rightarrow V'$  is hemicontinuous and bounded according to*

$$\|\mathcal{A}(t, v)\| \leq C(\|v\| + g(t)),$$

*for all  $v \in V$  and  $g \in L^2[0, t_m]$ ;*

- (iii) *there are real constants  $\alpha, \lambda > 0$  such that*

$$\mathcal{A}(t, v)v + \lambda \|v\|_H^2 \geq \alpha \|v\|_V^2,$$

*for almost every  $t \in [0, t_m]$  and  $v \in V$ .*

*Then, for every  $f \in \mathcal{V}'$  and  $u_0 \in H$ , there exists  $u \in \mathcal{V}$  such that*

$$\partial_t u(t) + \mathcal{A}(t, u(t)) = f(t) \in \mathcal{V}' \quad \text{and} \quad u(0) = u_0 \in H.$$

We remark that in [22], Showalter imposed the additional assumption that operator  $\mathcal{A}$  is monotone; however, this condition was only required for uniqueness of the solution, and we do not claim uniqueness here.

**2.2.2. Application to reduced model, with existence result.** For our simple reduced model that captures heat diffusion in a periodic array of ice bars immersed in water, the space  $V$  is equal to  $\mathcal{H}^1(\Omega_\varepsilon^1) \times \mathcal{H}^1(\Omega_\varepsilon^2)$  and hence the solution and test space  $\mathcal{V} = L^2([0, t_m], \mathcal{H}^1(\Omega_\varepsilon^1)) \times L^2([0, t_m], \mathcal{H}^1(\Omega_\varepsilon^2))$ . We also have that  $f \equiv 0 \in \mathcal{V}'$  and  $u_0 = (E_{1,\varepsilon}(0), E_{2,\varepsilon}(0))$ . The operator  $\mathcal{A}$  corresponding to the weak form of the problem (2.2) is

$$(2.5) \quad \begin{aligned} \mathcal{A}u(v) = & (D(u_1)\omega'(u_1)\nabla u_1, \nabla v_1)_{L^2(\Omega_\varepsilon^1)} + \varepsilon^2 \langle D(u_2)\omega'(u_2)\nabla u_2 \cdot \mathbf{n}, v_1 \rangle_{\mathcal{H}^{-\frac{1}{2}}(\Gamma_\varepsilon) \times \mathcal{H}^{\frac{1}{2}}(\Gamma_\varepsilon)} \\ & + \varepsilon^2 (D(u_2)\omega'(u_2)\nabla u_2, \nabla v_2)_{L^2(\Omega_\varepsilon^2)} \end{aligned}$$

where  $u = (u_1, u_2)$  and  $v = (v_1, v_2)$  are both in  $V$ . Notice that  $\mathcal{A}$  doesn't depend explicitly on time  $t$  and consequently hypothesis (i) in Showalter's Proposition is trivially satisfied. We may then restate the problem (2.4) as one of finding  $u = (E_{1,\varepsilon}, E_{2,\varepsilon}) \in (\mathcal{V}^1 + \omega^{-1}(T_a)) \times (\mathcal{V}^2 + E_{1,\varepsilon})$  such that

$$(2.6) \quad \begin{aligned} \int_0^{t_m} (\partial_t E_{1,\varepsilon}, \varphi)_{\Omega_\varepsilon^1} + (\partial_t E_{2,\varepsilon}, \psi)_{\Omega_\varepsilon^2} dt + \int_0^{t_m} (D(E_{1,\varepsilon})\omega'(E_{1,\varepsilon})\nabla E_{1,\varepsilon}, \nabla \varphi)_{L^2(\Omega_\varepsilon^1)} \\ + \varepsilon^2 \langle D(E_{2,\varepsilon})\omega'(E_{2,\varepsilon})\nabla E_{2,\varepsilon} \cdot \mathbf{n}, \varphi \rangle_{\mathcal{H}^{-\frac{1}{2}}(\Gamma_\varepsilon) \times \mathcal{H}^{\frac{1}{2}}(\Gamma_\varepsilon)} \\ + \varepsilon^2 (D(E_{2,\varepsilon})\omega'(E_{2,\varepsilon})\nabla E_{2,\varepsilon}, \nabla \psi)_{L^2(\Omega_\varepsilon^2)} dt = 0 \end{aligned}$$

for all  $\varphi, \psi \in V^1 \times V^2$ . To apply Showalter's Proposition, we take  $E_{1,\varepsilon}$  and  $E_{2,\varepsilon}$  equal to solution  $u$  and therefore adjust the function spaces by adding the Dirichlet conditions. We thereby obtain the differential operator  $\mathcal{A}$  used in our model, which we can show satisfies the remaining two conditions in Showalter's Proposition. We state this result as a Lemma whose proof is provided in Appendix A.

**LEMMA 2.2.** *The operator  $\mathcal{A} : V \rightarrow V'$  is*

- a) continuous,
- b) bounded, and
- c) coercive, in the sense that there are real constants  $\lambda, \alpha > 0$  such that

$$\mathcal{A}(t, v)(v) + \lambda \|v\|_H^2 \geq \alpha \|v\|_V^2,$$

for almost every  $v \in V$  and  $t \in [0, t_m]$ .

From continuity it follows immediately that  $\mathcal{A}$  is hemicontinuous. Therefore, we can apply Showalter's Proposition to obtain existence of a solution to the system (2.6).

**2.3. A priori estimates.** Our main results on a priori estimates are stated in Lemma 2.3 below, in which the functions  $E_{1,\varepsilon}$ ,  $T_{1,\varepsilon}$ , and  $E_{2,\varepsilon}$  and  $T_{2,\varepsilon}$  are bounded in  $L^2([0, t_m], \mathcal{H}^1(\Omega_\varepsilon^1))$  and  $L^2([0, t_m], \mathcal{H}^1(\Omega_\varepsilon^2))$  independent of  $\varepsilon$  (part a). Furthermore,  $D(E_{2,\varepsilon})\nabla T_{2,\varepsilon}$  must be bounded independent of  $\varepsilon$  in  $L^2([0, t_m], L^2(\Gamma_\varepsilon))$  (parts b,c) and there is also a strong convergence result for  $E_{1,\varepsilon}$  and  $E_{2,\varepsilon}$  in  $L^2([0, t_m], L^2(\Omega_\varepsilon^2))$  and  $L^2([0, t_m], L^2(\Omega_\varepsilon^1))$  respectively (parts d,e,f). The proof of this Lemma is given Appendix B.

LEMMA 2.3. *Here, the notation  $C_i$  represents a positive constant that is independent of  $\varepsilon$ .*

- a) *There exists a constant  $C_1$  such that*

$$\|T_{1,\varepsilon}\|_{\Omega_\varepsilon^1}^2 + \|\nabla T_{1,\varepsilon}\|_{\Omega_\varepsilon^1}^2 + \|T_{2,\varepsilon}\|_{\Omega_\varepsilon^2}^2 + \varepsilon^2 \|\nabla T_{2,\varepsilon}\|_{\Omega_\varepsilon^2}^2 \leq C_1.$$

- b) *There exists another constant  $C_2$  such that*

$$\|\nabla E_{1,\varepsilon}\|_{\Omega_\varepsilon^1}^2 + \|\nabla \cdot [D(E_{1,\varepsilon})\nabla T_{1,\varepsilon}]\|_{\Omega_{\varepsilon,t}^1}^2 + \varepsilon^2 \|\nabla E_{2,\varepsilon}\|_{\Omega_\varepsilon^2}^2 + \varepsilon^4 \|\nabla \cdot [D(E_{2,\varepsilon})\nabla T_{2,\varepsilon}]\|_{\Omega_{\varepsilon,t}^2}^2 \leq C_2.$$

- c) *There exists a constant  $C_3$  such that*

$$\varepsilon^3 \|D(E_{2,\varepsilon})\nabla T_{2,\varepsilon}\|_{\Gamma_{\varepsilon,t}}^2 \leq C_3.$$

- d) *The functions  $E_{1,\varepsilon}$ ,  $E_{2,\varepsilon}$  are nonnegative for almost every  $x \in \Omega_\varepsilon^1$ ,  $\Omega_\varepsilon^2$  as long as  $E_{1,\varepsilon}(0)$ ,  $E_{2,\varepsilon}(0)$  are nonnegative (respectively).*
- e) *There exists a constant  $C_4$  such that*

$$\|E_{1,\varepsilon}\|_{L^\infty(\Omega_\varepsilon^1)} + \|E_{2,\varepsilon}\|_{L^\infty(\Omega_\varepsilon^2)} \leq C_4.$$

- f) *There exists a constant  $C_5$  such that*

$$\|\partial_t E_{1,\varepsilon}\|_{L^2([0, t_m], L^2(\Omega_\varepsilon^1))} + \|\partial_t E_{2,\varepsilon}\|_{L^2([0, t_m], L^2(\Omega_\varepsilon^2))} \leq C_5.$$

Taking Lemma 2.3 along with the extension theorem in [17], we deduce that  $E_{1,\varepsilon}$  and  $E_{2,\varepsilon}$  are elements of  $L^2([0, t_m], \mathcal{H}^1(\Omega)) \cap \mathcal{H}^1([0, t_m], \mathcal{H}^{-1}(\Omega)) \cap L^\infty([0, t_m] \times \Omega)$ . An application of Lemma 5.6 of [12] then yields that  $E_{1,\varepsilon}$  and  $E_{2,\varepsilon}$  converge strongly in  $L^2([0, t_m], L^2(\Omega))$  to some functions  $E_{1,0}$  and  $E_{2,0}$  respectively. Because  $D$  is a continuous and bounded function, it then follows from the Theorem of Nemytskii [22, p. 48] that the function  $D : E_{i,\varepsilon} \mapsto D(E_{i,\varepsilon})$  is also continuous and bounded for  $i = 1, 2$ . Therefore, we conclude that  $D(E_{1,\varepsilon})$  and  $D(E_{2,\varepsilon})$  converge strongly in  $L^2([0, t_m], L^2(\Omega))$  to  $D(E_{1,0})$  and  $D(E_{2,0})$ , respectively.

Finally, because  $T_{1,\varepsilon} = \omega(E_{1,\varepsilon})$  where  $\omega$  is smooth, continuous and bounded (and similarly for  $\omega^{-1}$ ), we obtain that  $E_{1,\varepsilon}$  and  $T_{1,\varepsilon}$  both converge strongly in  $L^2([0, t_m], L^2(\Omega))$  and that  $T_{1,0} = \omega(E_{1,0})$ . An analogous result holds for  $T_{2,\varepsilon} = \omega(E_{2,\varepsilon})$ .

**2.4. Identification of the two-scale limit.** Armed with the fact that a solution of (2.2) exists for every  $\varepsilon > 0$ , and that the a priori estimates from the previous section hold, we know that the terms in Eqns. (2.2) two-scale converge to some limit (see [1, 20]). In order to investigate this limit, we define test functions that vary on length scales of size  $O(1)$  and  $O(\varepsilon)$  according to

$$\varphi_\varepsilon\left(x, \frac{x}{\varepsilon}\right) = \varphi_0(x) + \varepsilon \varphi_1\left(x, \frac{x}{\varepsilon}\right) \quad \text{and} \quad \psi_\varepsilon\left(x, \frac{x}{\varepsilon}\right),$$

where  $(\varphi_0, \varphi_1) \in C^\infty(\Omega) \times C^\infty(\Omega, C^\infty_\#(Y))$  and  $\psi_\varepsilon \in C^\infty(\Omega, C^\infty_\#(Y))$ , and the subscript  $\#$  denotes periodicity in space. We also need to introduce the characteristic functions

$$\chi^i\left(\frac{x}{\varepsilon}\right) = \begin{cases} 1, & \text{if } \frac{x}{\varepsilon} \in \Omega_\varepsilon^i, \\ 0, & \text{otherwise,} \end{cases}$$

for  $i = 1, 2$ . By substituting  $\varphi_\varepsilon$  into (2.2a) and using  $\chi^i$  to write the resulting integrals over the entire domain  $\Omega$ , we obtain

$$\begin{aligned} \int_{\Omega} \chi^1\left(\frac{x}{\varepsilon}\right) \partial_t E_{1,\varepsilon}(x, t) \varphi_\varepsilon\left(x, \frac{x}{\varepsilon}\right) dx + \int_{\Omega} \chi^1\left(\frac{x}{\varepsilon}\right) D(E_{1,\varepsilon}) \nabla T_{1,\varepsilon}(x, t) \nabla \varphi_\varepsilon\left(x, \frac{x}{\varepsilon}\right) dx \\ + \varepsilon^2 \int_{\Gamma_\varepsilon} D(E_{2,\varepsilon}) \nabla T_{2,\varepsilon}(x, t) \cdot \mathbf{n} \varphi_\varepsilon\left(x, \frac{x}{\varepsilon}\right) d\sigma_x = 0. \end{aligned}$$

Then, taking the limit as  $\varepsilon \rightarrow 0$  yields

$$\begin{aligned} (2.7) \quad \int_{\Omega \times Y^1} \partial_t E_{1,0}(x, t) \varphi_0(x) dy dx \\ + \int_{\Omega \times Y^1} D(E_{1,0}) [\nabla_x T_{1,0}(x, t) + \nabla_y \widehat{T}_{1,0}(x, y, t)] [\nabla_x \varphi_0(x) + \nabla_y \varphi_1(x, y)] dy dx \\ + \int_{\Omega \times \Gamma} D(E_{2,0}) \nabla_y T_{2,0}(x, y, t) \cdot \mathbf{n} \varphi_0(x) d\sigma_y dx = 0, \end{aligned}$$

where  $y$  denotes the variable that is defined on the reference cell  $Y$ . Note that  $T_{1,0} = \omega(E_{1,0}) \in L^2([0, t_m], \mathcal{H}^1(\Omega))$  is independent of  $y$ , and we have also introduced  $\widehat{T}_{1,0} \in L^2([0, t_m], L^2(\Omega, \mathcal{H}^1_\#(Y^1)))$  and  $T_{2,0} = \omega(E_{2,0}) \in L^2([0, t_m], L^2(\Omega, \mathcal{H}^1_\#(Y^2)))$ . The limit of  $\nabla T_{1,\varepsilon}$  has a special form proven in [1] that consists of two terms: one involving a gradient with respect to the slow variable, and a second term with respect to the fast variable. In a similar manner, we substitute the second test function  $\psi_\varepsilon$  into (2.2b) to get

$$\int_{\Omega} \chi^2\left(\frac{x}{\varepsilon}\right) \partial_t E_{2,\varepsilon}(x, t) \psi_\varepsilon\left(x, \frac{x}{\varepsilon}\right) dx + \varepsilon^2 \int_{\Omega} \chi^2\left(\frac{x}{\varepsilon}\right) D(E_{2,\varepsilon}) \nabla T_{2,\varepsilon}(x, t) \nabla \psi_\varepsilon\left(x, \frac{x}{\varepsilon}\right) dx = 0,$$

and again take the limit as  $\varepsilon \rightarrow 0$  to obtain

$$(2.8) \quad \int_{\Omega \times Y^2} \partial_t E_{2,0}(x, y, t) \psi_0(x, y) dy dx + \int_{\Omega \times Y^2} D(E_{2,0}) \nabla_y T_{2,0}(x, y, t) \nabla_y \psi_0(x, y) dy dx = 0.$$

We are free at this point to choose any test function, and so now we set  $\varphi_0 = 0$  in Eq. (2.7) and then introduce functions  $\mu_i \in \mathcal{H}^1_\#(Y^1)$  in order to express  $\widehat{T}_{1,0}(x, y, t) = \sum_{i=1}^n \partial_{x_i} T_{1,0}(x, t) \mu_i(y)$  in separable form. The weak formulation of the cell problem for  $i = 1, \dots, n$  may then be expressed in the much simpler form

$$(2.9) \quad (e_i + \nabla_y \mu_i, \nabla_y \varphi_1)_{Y^1} = 0,$$

where  $\mu_i$  is  $Y$ -periodic. Alternately, we may take  $\varphi_1 = 0$  in Eq. (2.7) to obtain

$$\begin{aligned} \int_{\Omega \times Y^1} \partial_t E_{1,0}(x, t) \varphi_0(x) dy dx + \int_{\Omega \times Y^1} D(E_{1,0}) \sum_{i=1}^n \partial_{x_i} T_{1,0}(x, t) [e_i + \nabla_y \mu_i(y)] \nabla_x \varphi_0(x) dy dx \\ + \int_{\Omega \times \Gamma} D(E_{2,0}) \nabla_y T_{2,0}(x, y, t) \cdot \mathbf{n} \varphi_0(x) d\sigma_y dx = 0, \end{aligned}$$

which can be rewritten in the more suggestive form

$$\begin{aligned} (2.10) \quad \int_{\Omega \times Y^1} \partial_t E_{1,0}(x, t) \varphi_0(x) dy dx + \int_{\Omega} D(E_{1,0}) \sum_{i,j=1}^n \partial_{x_i} T_{1,0}(x, t) \int_{Y^1} [\delta_{ij} + \partial_{y_j} \mu_i(y)] dy \partial_{x_j} \varphi_0(x) dx \\ + \int_{\Omega \times \Gamma} D(E_{2,0}) \nabla_y T_{2,0}(x, y, t) \cdot \mathbf{n} \varphi_0(x) d\sigma_y dx = 0. \end{aligned}$$



The diffusion term involves the extra factors

$$(2.11) \quad \Pi_{ij} = \int_{Y^1} (\delta_{ij} + \partial_{y_j} \mu_i) dy$$

for  $i, j = 1, \dots, n$  which can be represented as a matrix  $\Pi$  that multiplies the diffusion coefficient  $D(E_{1,0})$ . Hence, we obtain the limit equations from (2.8) and (2.10)

$$(2.12a) \quad |Y^1|(\partial_t E_{1,0}, \varphi)_\Omega + (\Pi D(E_{1,0}) \nabla_x T_{1,0}, \nabla_x \varphi)_\Omega + (D(E_{2,0}) \nabla_y T_{2,0} \cdot \mathbf{n}, \varphi)_{\Omega \times \Gamma} = 0,$$

$$(2.12b) \quad (\partial_t E_{2,0}, \psi)_{\Omega \times Y^2} + (D(E_{2,0}) \nabla_y T_{2,0}, \nabla_y \psi)_{\Omega \times Y^2} = 0,$$

for all  $\varphi \in \mathcal{H}^1(\Omega)$  and  $\psi \in L^2(\Omega, \mathcal{H}_\#^1(Y^2))$ , where  $\Pi$  is the  $n \times n$  matrix of scaling factors defined in (2.11),  $T_{1,0} \in L^2([0, t_m], \mathcal{H}^1(\Omega))$  with  $T_{1,0} = T_a$  on  $\partial\Omega$ , and  $T_{2,0} \in L^2([0, t_m], L^2(\Omega, \mathcal{H}_\#^1(Y^2)))$  with  $T_{2,0} = T_{1,0}$  on  $\Omega \times \Gamma$ .

To simplify notation in the remainder of the paper, we drop the zero subscripts in  $(T_{1,0}, E_{1,0}, T_{2,0}, E_{2,0})$  and denote them instead by  $(T_1, E_1, T_2, E_2)$ .

**2.5. Uniqueness.** The uniqueness of the solution to equations (2.12) may be formulated compactly in terms of the following lemma, which is proven in Appendix C.

LEMMA 2.4. *Equations (2.12) have at most one solution given by*

$$\begin{aligned} T_1 &\in \mathcal{V}^1(\Omega) + T_a = L^2([0, t_m], \mathcal{H}_0^1(\Omega)) \cap \mathcal{H}^1([0, t_m], L^2(\Omega)) + T_a, \\ T_2 &\in \mathcal{V}^2(\Omega \times Y^2) + T_1 = L^2([0, t_m], L^2(\Omega, \mathcal{H}_\#^1(Y^2))) \cap \mathcal{H}^1([0, t_m], L^2(\Omega \times Y^2)) + T_1, \end{aligned}$$

where  $T_1 = \omega(E_1)$  and  $T_2 = \omega(E_2)$ .

**2.6. Strong formulation of the limit problem.** We now state an equivalent strong formulation of the limit problem corresponding to the weak form in Eqs. (2.12), which consists of a PDE for  $E_1$  on the entire domain  $\Omega$

$$\begin{aligned} |Y^1| \partial_t E_1 - \nabla_x \cdot (\Pi D(E_1) \nabla_x T_1) &= \int_\Gamma D(E_2) \nabla_y T_2 \cdot \mathbf{n} d\sigma_y && \text{in } \Omega, \\ T_1 &= T_a && \text{on } \partial\Omega, \end{aligned}$$

along with a second PDE for  $E_2$  on  $\Omega \times Y^2$

$$\begin{aligned} \partial_t E_2 - \nabla_y \cdot (D(E_2) \nabla_y T_2) &= 0 && \text{on } \Omega \times Y^2, \\ T_2 &= T_1 && \text{on } \Omega \times \Gamma, \end{aligned}$$

along with suitable initial values for enthalpy that we denote  $E_{1,init}$  and  $E_{2,init}$ . These two problems are coupled through the temperature function  $T_2$  via an integral term and the final boundary condition, both of which are enforced on  $\Gamma$ . This is known as the *two-phase formulation of the Stefan problem*, for which there is no explicit equation for the motion of the phase interface; instead, the interface location is captured implicitly through the function  $T = \omega(E)$ .

Under suitable assumptions (see [24]) the above problem may be rewritten in an equivalent *one-phase formulation* consisting of the same equation for the enthalpy  $E_1$  on the macroscale

$$(2.13a) \quad |Y^1| \partial_t E_1 - \nabla_x \cdot (\Pi D(E_1) \nabla_x T_1) = \int_\Gamma D(E_2) \nabla_y T_2 \cdot \mathbf{n} d\sigma_y \quad \text{in } \Omega,$$

$$(2.13b) \quad T_1 = T_a \quad \text{on } \partial\Omega,$$

along with the following equations for temperature on the reference cell

$$(2.14a) \quad c_w \partial_t T_2 - \nabla_y \cdot (D(E_2) \nabla_y T_2) = 0 \quad \text{on } \Omega \times \tilde{Y}^2(x, t),$$

$$(2.14b) \quad T_2 = T_1 \quad \text{on } \Omega \times \Gamma,$$

$$(2.14c) \quad T_2 = T_c \quad \text{on } \Omega \times \partial\tilde{Y}^2(x, t).$$



These equations are supplemented by an evolution equation for the phase boundary

$$(2.15) \quad \partial_t s = -\frac{D(E_2)}{(E_w - E_i)} \nabla_y T_2 \cdot \mathbf{n} \quad \text{on } \Omega \times \partial \tilde{Y}^2(x, t),$$

where the ice/water interface is denoted  $\partial \tilde{Y}^2(x, t)$  and depends on both  $x$  and  $t$  because the domains may differ in  $\Omega \times [0, t_m]$ . Note that in this one-phase formulation the temperature is only defined within the portion of the domain that contains water (for freezing) or ice (for thawing). Furthermore, we obtain an explicit equation (2.15) governing the dynamics of the location  $s(x, y, t)$  of the phase interface, which is known as the *Stefan condition*. When performing numerical simulations of the limit problem, it is most convenient to employ the one-phase formulation of the Stefan problem.

### 3. Numerical simulations of the homogenized problem.

**3.1. Description of the numerical algorithm.** We now develop an algorithm for computing the solution  $E_1(x, t)$ ,  $T_2(x, y, t)$  and  $s(x, y, t)$  to the one-phase Stefan problem (2.13)–(2.15), which also requires values of the coefficients  $\Pi_{ij}$  from the reference cell problem (2.9). We consider only 2D simulations in this paper, although the algorithm extends naturally to three dimensions. Our approach is a simple one that is based on three key approximations:

- The coefficients  $\Pi_{ij}$  are defined on the reference cell and are in fact constants that are independent of temperature and interface location. Consequently, these coefficients only need to be computed once at the beginning of a simulation.
- The reduced model has an inherent radial symmetry on the microscopic scale, and so we restrict ourselves in this paper to problems that have an analogous radial symmetry on the macroscale; this is natural for the application to a tree cross-section considered in Section 4. Consequently, all variables and governing equations are recast in terms of a single radial coordinate (which we continue to label as  $x$  or  $y$ ) so that only one-dimensional problems are solved at both the micro- and macroscale.
- Because of the simple form of the coupling between microscale and macroscale problems that involves only interfacial solution values, we propose a simple “frozen coefficient” splitting approach for time-stepping in which each variable is advanced to the next time step individually, holding all other variables constant at their previous values.

With this in mind, we can now summarize our multiscale numerical algorithm as follows. We use a method-of-lines approach in which the unknowns are discretized in space (radius) and then the resulting coupled system of ordinary differential equations is integrated in time using a stiff ODE solver. In particular, we have implemented our algorithm in *Matlab* and employed the solver *ode15s*. Because our ultimate goal is to simulate sap flow in a tree stem having a circular cross-section, we consider a problem domain  $\Omega$  that is a circle with some given radius  $R_{tree}$ . The spatial discretization is then performed on two distinct scales:

- the *macroscale* corresponding to the circular domain  $\Omega$ , that is divided into an equally-spaced grid of  $M$  radial points at each of which we have unknown values of  $E_1$ ,  $T_1$  and  $s$ ; and
- the *microscale* corresponding to the reference cell  $Y$ , which is solved for  $T_2$  and  $E_2$  at each macroscale point. The local ice region  $\tilde{Y}^2$  grows or shrinks in time according to the local phase boundary location  $s$ . Therefore, we use a *moving mesh* approach wherein the reference cell is discretized at a set of  $m$  equally-spaced radial points that move in time as the ice/water phase interface moves. In practice, it is sufficient to use a coarse grid here with  $m \ll M$ .

The algorithm now proceeds according to the following steps.

- Step 1: Set initial values of  $T_2 = T_{2,init}$  at each macroscale point, while  $E_1 = E_{1,init}$  and  $s = s_{init}$  within each local reference cell.
- Step 2: For a single canonical reference cell that takes the shape of a square with a circular hole, we use *COMSOL* to approximate the functions  $\mu_i(y)$  from the integral equation (2.9) and to calculate the integral. This yields precomputed values of the four entries of matrix  $\Pi$  that are used in the remainder of the computation.
- Step 3: At each time step, advance the solution components as follows:
- 3a. Set  $T_1 = \omega(E_1)$  and  $E_2 = \omega^{-1}(T_2)$ .

TABLE 1  
Values of parameters in the reduced model for melting ice bars, taken from [5].

Symbol	Description	Value	Units
$c_w$	Specific heat of water	4180	$J/kg^\circ K$
$c_i$	Specific heat of ice	2100	$J/kg^\circ K$
$E_w$	Enthalpy of water at $T_c$	$9.07 \times 10^5$	$J/kg$
$E_i$	Enthalpy of ice at $T_c$	$5.74 \times 10^5$	$J/kg$
$k_w$	Thermal conductivity of water	0.556	$W/m^\circ K$
$k_i$	Thermal conductivity of ice	2.22	$W/m^\circ K$
$\rho_w$	Density of water	1000	$kg/m^3$
$\rho_i$	Density of ice	917	$kg/m^3$
$T_c$	Melting (critical) temperature	273.15	$^\circ K$
$T_a$	Ambient (outside) temperature	$T_c + 10$	$^\circ K$
$T_{init}$	Initial temperature	$T_c$	$^\circ K$
$\delta$	Length of reference cell	$1.0 \times 10^{-3}$	$m$
$\gamma$	Radius of artificial boundary $\Gamma$	$0.45 \delta$	$m$

- 3b. Discretize the microscale heat equation problem (2.14) in space on each local cell  $\tilde{Y}^2(x, t)$  within the annular-shaped water region only by using a moving spatial grid with points  $y_j = s + j(\gamma - s)/m$  for  $j = 0, 1, \dots, m$  (the ice region has known constant temperature  $T_1 \equiv T_c$  and so no discretization is required there). A finite element approximation is used with linear Lagrange elements as basis functions, and the solution is integrated over a single time step by freezing the values of  $E_1$ ,  $T_1$  and  $s$  at the previous step. In practice, sufficient accuracy is obtained by taking  $m = 4$ .
- 3c. Integrate the macroscale problem (2.13) for  $E_1$  at the fixed grid points  $x_i = iR_{tree}/M$  for  $i = 0, 1, \dots, M - 1$ . Due to the radial symmetry of the domain  $Y^2$ , the integral in (2.13a) reduces to  $2\pi r D(E_2) \nabla T_2 \cdot \mathbf{n}$  where  $r$  is the radius of  $Y^2$ . Again, we use a finite element discretization in space with linear Lagrange elements, this time freezing  $E_2$  and  $T_2$  at the current values. Note that here is where the precomputed values of  $\Pi_{ij}$  are required from the reference cell.
- 3d. Integrate the interface evolution equation (2.15) by using a finite difference approximation of the derivative in the right hand side, and by freezing values of  $T_2$  at the current time.
- 3e. Increment the time variable and return to Step 3a.

The above algorithm must be modified when the ice completely melts and the governing equations change in that the interface location  $s$  becomes identically zero and the Stefan condition (2.15) drops out. At the same time, the separation of the reference cell into two sub-domains  $Y^1$  and  $Y^2$  (which is required to handle the Dirichlet condition on temperature at the phase interface) is no longer necessary and hence the temperature can be described by the single field  $T_1$  that obeys (2.13) alone (with zero right hand side, constant  $D$ , and  $\Pi \equiv 1$ ). This alteration to the governing equations can be handled easily in the numerical algorithm above by a form of “event detection” based on the ice bar radius  $s$ : when  $s > 0$ , ice is still present and the original equations are solved; but as soon as  $s = 0$ , ice is totally melted and the modified equations just described are solved instead (omitting steps 3b and 3d).

**3.2. Numerical results.** We now present numerical simulations of the reduced model wherein a periodic array of ice bars is suspended within a circular water-filled domain. The domain has a radius of  $R_{tree} = 0.25 m$  and the periodic reference cell  $Y = [0, \delta]^2$  depicted in Figure 1 is given a size  $\delta = 10^{-3} m$ . The system is solved in dimensional variables so that there is no need to non-dimensionalize and hence the size of the reference cell is simply equal to the physical dimension  $\delta$ . We assume that the ice bars each have initial radius  $s(0) = 0.1 \delta = 10^{-4} m$  and we take the radius of the artificial boundary  $\Gamma$  in the reference cell to be  $\gamma = 0.45 \delta$ . All other physical parameter values are listed in Table 1.

Figure 3 presents snapshots at a number of time points that show the variation in global temperature  $T_1$  and the radius of the ice bars  $s$  throughout the domain. As time goes on, the temperature gradually increases as heat from the outer boundary diffuses inwards. In response to this rise in temperature, the ice melts and the size of the ice bar in each local cell problem decreases. The ice in the outermost regions melts first and

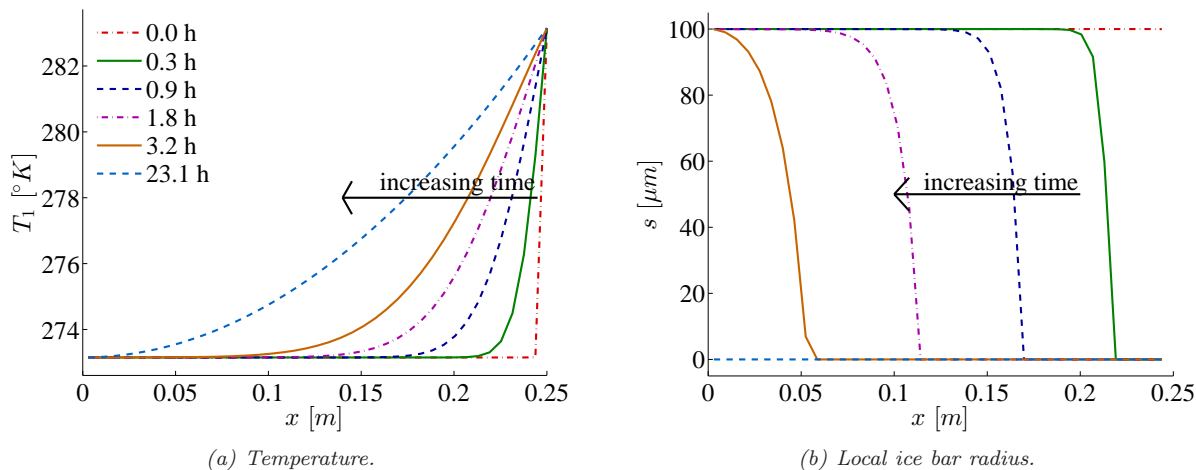


FIGURE 3. Solution profiles for the local problem, shown at selected times between 0 and 23 h.

by time  $t \approx 23h$ , the entire domain is completely melted. In contrast with the results in [5] that present the progress of thawing at some specific location on the microscale, these results illustrate the progress of the thawing front on the macroscale.

**4. Application to maple sap exudation.** Our aim is now to apply the limit problem (2.13) and (2.14) to the study of sap exudation in maple trees, which was the original motivation for developing the periodic homogenization analysis in this paper. Sugar maple trees (along with a few other relatives such as black maple, birch, walnut and sycamore) have a unique ability amongst all tree species in that they exude large quantities of sap during the winter in the leafless state. Sap exudation is driven by an elevated pressure in the tree stem that builds up over a period of several days in which air temperature oscillates above and below the freezing point. The ability of maple to exude sap has intrigued tree physiologists for nearly a century, and various physical and biological processes have been proposed to explain this behaviour [14, 18, 23]. Although a significant degree of controversy remains over the root causes of sap exudation the most plausible and widely-accepted explanation is a freeze/thaw hypothesis proposed by Milburn and O'Malley [19]. The first complete mathematical model of the physical processes underlying their hypothesis was developed by Ceseri and Stockie[5], who focused on the thawing half of the cycle.

**4.1. Physical background: The Milburn-O'Malley process.** The Milburn-O'Malley process depends integrally on the distinctive microstructure of the sapwood (or xylem) in sugar maple trees (*Acer saccharum*). Wood in most deciduous tree species consists of long, straight, roughly cylindrical cells that are on the order of 1 mm long. These cells can be classified into two main types: *vessels* having an average radius of 20  $\mu\text{m}$ , which are surrounded by the much more numerous (*libriform*) *fibers* with a radius of roughly 3–4  $\mu\text{m}$ . The repeating structure of vessels and fibers is illustrated in Figure 4. The vessels, being significantly larger, provide the main route for transport of sap from roots to leaves during the growing season whereas the fibers are understood to play a largely passive structural role. Under normal conditions the vessels are filled with sap, which is mostly made up of water but can also contain as much as 2–3% sugar by weight for species like the sugar maple. On the other hand, fibers are thought to be primarily filled with gas (i.e., air) and there is often also gas present within the vessel sap either as bubbles or in dissolved form.

Milburn and O'Malley hypothesized that during late winter when evening temperatures begin to drop and just before the onset of freezing, sap is drawn through tiny pores in the fiber/vessel walls by capillary and adsorption forces into the gas-filled fibers where it begins to freeze on the inner surface of the fiber wall (refer to Figure 4(b), top “cooling sequence”). As temperatures drop further the ice layer grows and the gas trapped inside is compressed, forming a pressure reservoir. When temperatures again rise above freezing the next day, the process reverses: the ice layer melts and the pressurized gas drives liquid melt-water back into the vessel where it then (re-)pressurizes the vessel compartment (the “warming sequence” in Figure 4(b)). Milburn and O'Malley also stressed the importance of incorporating osmotic effects in order to obtain the

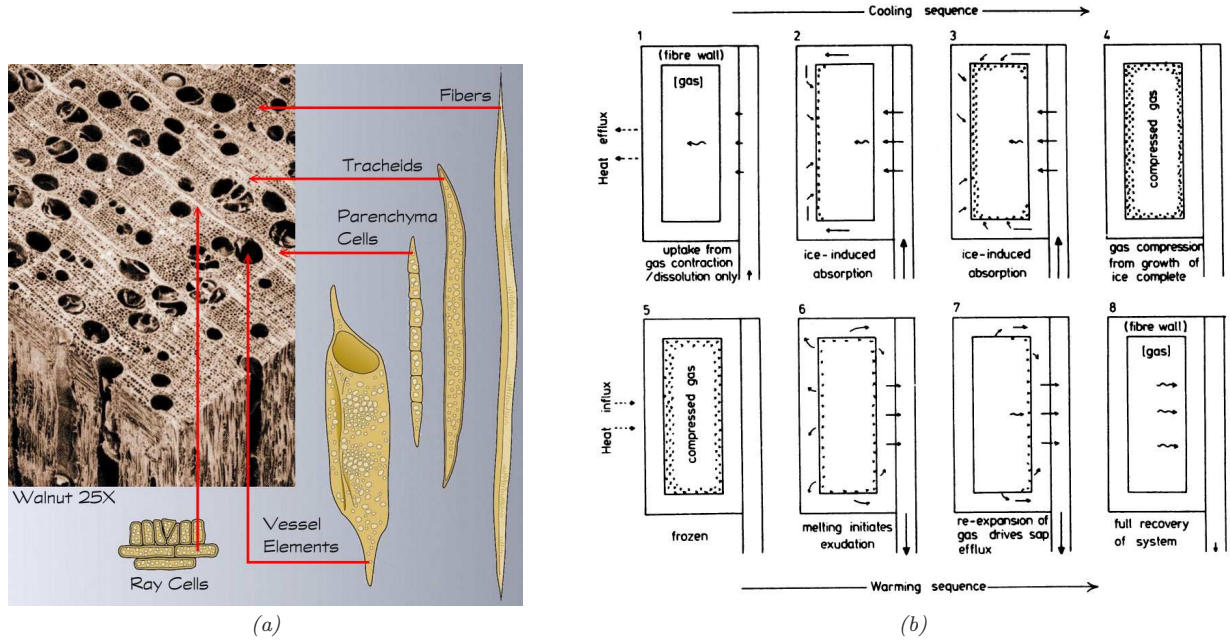


FIGURE 4. (a) A cut-away view of the sapwood (or xylem) in a hardwood tree such as sugar maple, illustrating the repeating microstructure of vessels surrounded by fibers (the other cell types indicated here are ignored in our model). Source: Workshop Companion [27]. (b) Illustration of the Milburn-O'Malley process taken from [19, Fig. 7] (© 2008 Canadian Science Publishing, reproduced with permission). Our focus is the “warming sequence” in the bottom row, numbers 5–8. The fiber is the large rectangular structure on the left of each image and the vessel is represented by a vertical channel on the right (not drawn to scale).

high sap pressures actually observed in sugar maple trees, and this has since been verified in experiments [7]. The osmotic pressure derives from the selectively permeable nature of the fiber/vessel wall, which prevents sugars in the vessel sap from entering the fiber and thereby introduces an osmotic pressure gradient between the sugar-rich vessel sap and the pure water contained in the fiber. The presence of sugar also leads to a freezing point depression effect in which the vessel sap has a lower freezing point than the fiber water.

There are two additional features not included in [19] that are essential in order to obtain physically relevant results. First of all, Ceseri and Stockie [5] demonstrated the necessity of including gas bubbles within the vessel sap in order to permit exchange of pressure between the vessel and fiber compartments. Secondly, despite the pervading belief that there is no significant root pressure in maple during winter [15, 26], we found to the contrary that it is essential to include uptake of root water during the freezing process in order that pressure can accumulate over multiple freeze/thaw cycles. Indeed, this second addition is supported by the recent experiments of Perkins and van den Berg [4] that demonstrate the existence of significant root pressures during the sap harvest season.

**4.2. Mathematical formulation.** The physical description of the modified Milburn-O'Malley hypothesis outlined in the previous section (with the exception of the root pressure) was used in [5] to derive a mathematical model for the cell-level processes driving sap exudation over a single freezing cycle. Our reduced model for melting ice bars described in Section 2 captures the phase change aspects of this process, with the ice bars being analogous to regions of frozen water contained within fiber cells in the sapwood. However, we need to add a number of extensions to the reduced model in order to capture the remainder of the physics inherent in sap exudation:

1. *Introduce a gas phase:* which takes the form of a gas bubble in both fiber and vessel and implies that the diffusion coefficient varies in space. Although we do not provide the analytical derivation for this more general class of diffusion coefficient, the extension of our analysis is straightforward.
2. *Dissolved sugar in the vessel sap:* which gives rise to an osmotic potential between fiber and vessel that is essential for generating realistic exudation pressures. Sugar within the vessel sap also depresses

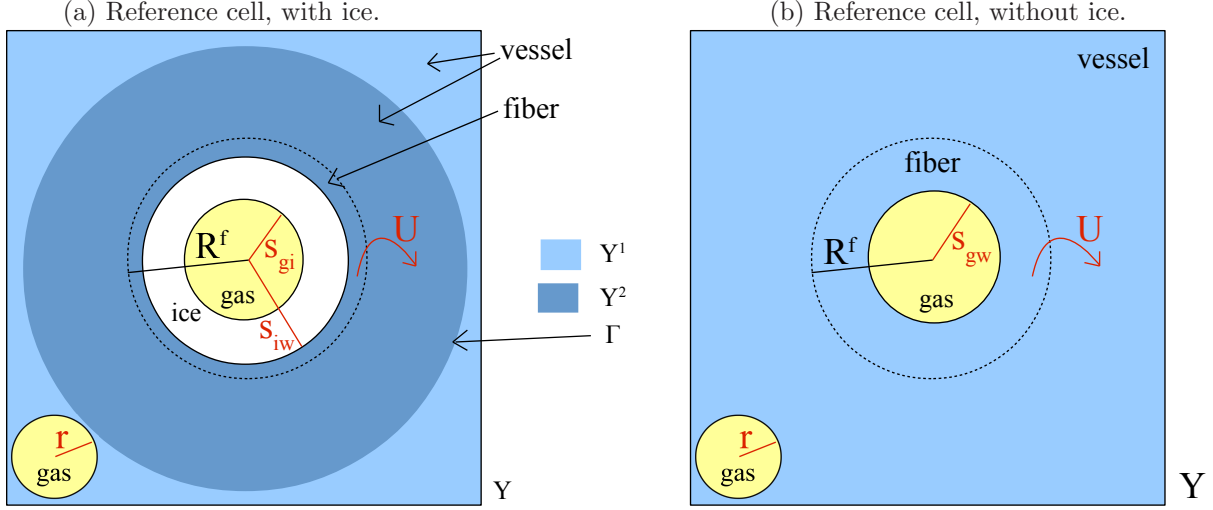


FIGURE 5. Geometry of the reference cell for the maple sap exudation problem. (a) Initially, the vessel compartment contains a gas bubble with radius  $r$ , while the circular fiber (radius  $R^f$ ) contains a gas bubble (radius  $s_{gi}$ ), surrounded by an ice layer (thickness  $s_{iw} - s_{gi}$ ), and finally a layer of melt-water (thickness  $R^f - s_{iw}$ ). The porous wall between fiber and vessel is denoted by a dotted line. As ice melts, the melt-water is forced out by gas pressure through the porous fiber wall into the surrounding vessel compartment. The total volume of melt-water transferred from fiber to vessel is denoted  $U$ . (b) After the ice has completely melted, the problem simplifies significantly leaving only a single interface ( $s_{gw}$ , between gas/water) and a single temperature field  $T_1$  for the domain  $Y \equiv Y^1$ .

the freezing point so that the function  $\omega$  in (2.1) differs between vessel and fiber. Although we do not need to incorporate freezing point depression explicitly in our model, it could be handled in several ways, for example by adding an extra spatial dependence in  $\omega$ . Alternatively, the fiber could be defined as separate domain that is connected to the vessel via appropriate boundary conditions, thereby ensuring that the homogenization results carry through for the sap exudation model. We have therefore chosen not to present the analytical derivation for this case, although various possible functional forms for  $\omega$  can be found in [3].

3. *Permeability of the cell wall to water:* which permits the fiber/vessel pressure exchange and also sets up the sugar concentration difference that drives osmosis. This in turn introduces an additional term in equation (2.15) (for the strong formulation) that governs the dynamics of the ice/water interface.

Although we do take the necessary step of including the gas phase in both cell chambers (fiber and vessel) we assume for the sake of simplicity that the effects of gas dissolution and nucleation are negligible. This is the primary difference between our microscale model and the model in [5] on which it is based, although re-introducing gas dissolution effects would certainly be an interesting topic for future research.

With the above modifications in mind, we consider the modified reference cell geometry pictured in Figure 5a wherein a circular fiber of radius  $R^f$  is located adjacent to a vessel compartment. The fiber is subdivided into nested annular regions containing gas, ice and liquid, and the outer radii of the phase interfaces are denoted  $s_{gi}$  (for gas/ice) and  $s_{iw}$  (for ice/water). The vessel also contains a circular gas bubble of radius  $r$ . One additional time-dependent variable is introduced to measure the total volume of water transferred from fiber to vessel, denoted  $U$ . These four variables depend on time  $t$  and also on the position  $x$  of the reference cell in space. The region lying outside the fiber and inside the boundary of the square reference cell represents the sap-filled vessel. Although the shape of this vessel region clearly does not correspond to the cylindrical shape of real vessels, we argue that it is nonetheless a reasonable approximation considering that the vessel is so much larger than the fiber. This reference cell geometry should be contrasted with that used in [5, Fig. 3.1].

We are now prepared to describe the governing equations for the homogenized sap exudation problem. The domain of interest  $\Omega$  is a 2D circular cross-section of a tree stem. At every point in  $\Omega$  is associated a reference cell  $Y$ , and hence the actual domain of interest consists of  $\Omega \times Y$ . In comparison with the reduced problem studied in Section 2, the sap exudation problem includes additional phases that need to



be incorporated into the local/global temperatures as well as the phase interfaces, as described under points 1–3 above. The equations for temperature are similar to those for the reduced model so that the periodic homogenization results require no significant changes. Therefore, the same limit problem (2.13) and (2.14) derived earlier for the reduced model may also be used for the maple sap exudation application, with Eq. (2.15) replaced by Eq. (4.1a).

For the reference cell problem, the dynamics for  $s_{iw}$ ,  $s_{gi}$ ,  $r$  and  $U$  are governed by four differential equations whose derivation can be found in [5]:

$$(4.1a) \quad \partial_t s_{iw} = -\frac{D(E_2)}{E_w - E_i} \nabla_y T_2 \cdot \mathbf{n} + \frac{1}{2\pi s_{iw} L^f} \partial_t U, \quad (\text{Stefan condition})$$

$$(4.1b) \quad 0 = -\rho_i s_{gi} \partial_t s_{gi} + (\rho_i - \rho_w) s_{iw} \partial_t s_{iw} + \frac{1}{2\pi L^f} \partial_t U, \quad (\text{conservation of mass})$$

$$(4.1c) \quad \partial_t r = \frac{N}{2\pi r L^v} \partial_t U, \quad (\text{conservation of volume})$$

$$(4.1d) \quad \partial_t U = -\frac{KA}{N\rho_w g W} (p_w^v - p_w^f - \mathcal{R}C_s T_1). \quad (\text{Darcy's law and osmotic pressure})$$

Here we have introduced new variables for pressure  $p$  and density  $\rho$ , and the superscripts  $f/v$  refer to fiber/vessel while subscripts  $g/i/w$  refer to gas/ice/water phases. We make particular note of the fact that in sapwood there are many more fibers than vessels (see Figure 4a) and so the effect of any fiber-vessel flux terms must be increased to take into account the multiplicity of the fibers. With this in mind, we have introduced the parameter  $N$  in (4.1c)–(4.1d) that represents the average number of fibers per vessel, and for which we choose  $N = 16$ . Note also that in the Stefan condition (4.1a) for the motion of the ice/water interface we have incorporated an additional term  $\partial_t U / (2\pi s_{iw} L^f)$  that was neglected in [5] and serves to capture the change in fiber water volume due to outflow through the fiber/vessel wall.

Also appearing in (4.1) are several intermediate variables that are given by the following algebraic relations

$$(4.2a) \quad p_w^f = p_g^f(0) \frac{s_{gi}(0)^2}{s_{gi}^2} - \frac{\sigma_w}{s_{gi}}, \quad (\text{Young-Laplace equation for fiber})$$

$$(4.2b) \quad p_w^v = p_g^v - \frac{\sigma_w}{r}, \quad (\text{Young-Laplace equation for vessel})$$

$$(4.2c) \quad p_g^v = \frac{\rho_g^v \mathcal{R} T_1}{M_g}, \quad (\text{ideal gas law for vessel})$$

$$(4.2d) \quad \rho_g^v = \frac{\rho_g^v(0) V_g^v(0)}{V_g^v + H(V^v - V_g^v)}, \quad (\text{density-volume correlation})$$

$$(4.2e) \quad V_g^v = \pi r^2 L^v, \quad (\text{volume of gas in vessel})$$

where  $V$  represents volume. All other quantities appearing in the above equations that have not been introduced previously correspond to constant parameters whose definitions and numerical values are listed in Table 2.

In any given reference cell, a thawing scenario will eventually reach a time when the fiber ice layer is completely melted, for which the reference cell is pictured in Figure 4b. In the absence of ice, the macroscale equations remain unchanged but the microscale problem must be modified in a manner very similar to what we did for the reduced problem at the end of Section 3.1. In the sap exudation case the diffusion coefficient  $D$  must account for the fact that there are two possible values, one in the gas region and one in the water-filled region. Furthermore, the microscale equation for the ice/water interface (4.1a) drops out and we identify  $s_{iw} \equiv s_{gi} =: s_{gw}$ , where the latter refers to the new fiber gas/water interface. This leads to a slight simplification in (4.1b) since the two time-derivative terms involving  $\rho_i$  cancel. Otherwise, the microscale equations (4.1) and (4.2) remain the same.

**4.3. Simulations of maple sap exudation.** A tree stem is roughly a right circular cylinder, and so we employ in our numerical simulations a macroscopic domain  $\Omega$  consisting of a 2D horizontal stem cross-section in the shape of a circle of radius  $R_{tree}$ . Because of radial symmetry, we therefore have a one-dimensional

TABLE 2

Constant parameter values and initial conditions used in the sap exudation model, with most values taken from [5].

<i>Symbol</i>	<i>Description</i>	<i>Value</i>	<i>Units</i>
$\delta$	Length of reference cell	$3.60 \times 10^{-5}$	$m$
$R^f$	Fiber radius	$3.5 \times 10^{-6}$	$m$
$L^v$	Vessel length	$5.0 \times 10^{-4}$	$m$
$L^f$	Fiber length	$1.0 \times 10^{-3}$	$m$
$V^f$	Fiber volume $= \pi(R^f)^2 L^f$	$3.85 \times 10^{-14}$	$m^3$
$V^v$	Vessel volume $= \delta^2 L^v - V^f$	$6.10 \times 10^{-13}$	$m^3$
$A$	Fiber surface area $= 2\pi R^f L^f$	$2.20 \times 10^{-8}$	$m^2$
$W$	Thickness of fiber/vessel wall	$3.64 \times 10^{-6}$	$m$
$N$	Number of fibers per vessel	16	
$R_{tree}$	Tree radius	0.25	$m$
$g$	Gravitational acceleration	9.81	$m/s^2$
$H$	Henry's constant	0.0274	—
$M_g$	Molar mass of air	0.029	$kg/mol$
$\mathcal{R}$	Gas constant	8.314	$J/mol^\circ K$
$\sigma_w$	Water surface tension	0.076	$N/m$
$C_s$	Vessel sugar concentration	58.4	$mol/m^3$
$K$	Wall hydraulic conductivity	$1.98 \times 10^{-14}$	$m/s$
$T_c$	Melting temperature	273.15	$^\circ K$
$T_a$	Ambient temperature $= T_c + 10$	283.15	$^\circ K$
$T_{init}$	$= T_c$	273.15	$^\circ K$
$s_{iw}(0)$	$= R^f$	$3.5 \times 10^{-6}$	$m$
$s_{gi}(0)$	$= R^f/\sqrt{2}$	$2.5 \times 10^{-6}$	$m$
$r(0)$		$6.0 \times 10^{-6}$	$m$
$U(0)$		0	$m^3$
$p_g^f(0)$		$2.0 \times 10^5$	$N/m^2$
$p_g^v(0)$		$1.0 \times 10^5$	$N/m^2$
$p_w^f(0)$		$9.89 \times 10^4$	$N/m^2$
$p_w^v(0)$		$9.95 \times 10^4$	$N/m^2$

problem that varies only in the radial direction. We take a representative value of  $R_{tree} = 0.25 \text{ m}$  and choose the length of the reference cell to be  $\delta = 3.60 \times 10^{-5} \text{ m}$ . The initial temperature of the tree is taken to be  $T_{init} = 0^\circ C$  throughout, with the fiber water initially frozen and the vessel water in liquid form owing to the freezing point depression effect. There is no need to explicitly incorporate this effect into the model since we are only concerned with the thawing process, where the initial temperature is at the melting point of pure water; hence, the only impact of freezing point depression in this paper is on the initial conditions in that the vessel water is initially in liquid form. The outer boundary of the tree stem is held equal to an ambient temperature  $10^\circ C$  above the freezing point, corresponding to  $T_1(0.25, t) = T_a = T_c + 10$ , while the symmetry condition  $\partial_x T_1(0, t) = 0$  is imposed at the center of the domain. All parameters that are common to the reduced model are listed in Table 1 and their values remain the same, whereas any new parameters introduced in the sap exudation model are listed in Table 2.

We remark that a Robin boundary condition (or convective heat transport condition) is a more appropriate condition to impose at the outer tree surface. However, we have chosen to use a Dirichlet boundary condition here because it is consistent with the homogenized problem derived in Section 2. The extension to the Robin condition is actually quite straightforward to implement numerically, but it is a major extension to our analysis and so we relegate it to future work.

We now give a brief description of our numerical solution algorithm, which solves the coupled system of governing equations using a split-step approach that alternates between solving the microscale (reference cell) and macroscale solutions. First, the microscale problem consisting of the differential-algebraic system (2.14) and (4.1) is solved using a finite element discretization analogous to what we employed for the reduced



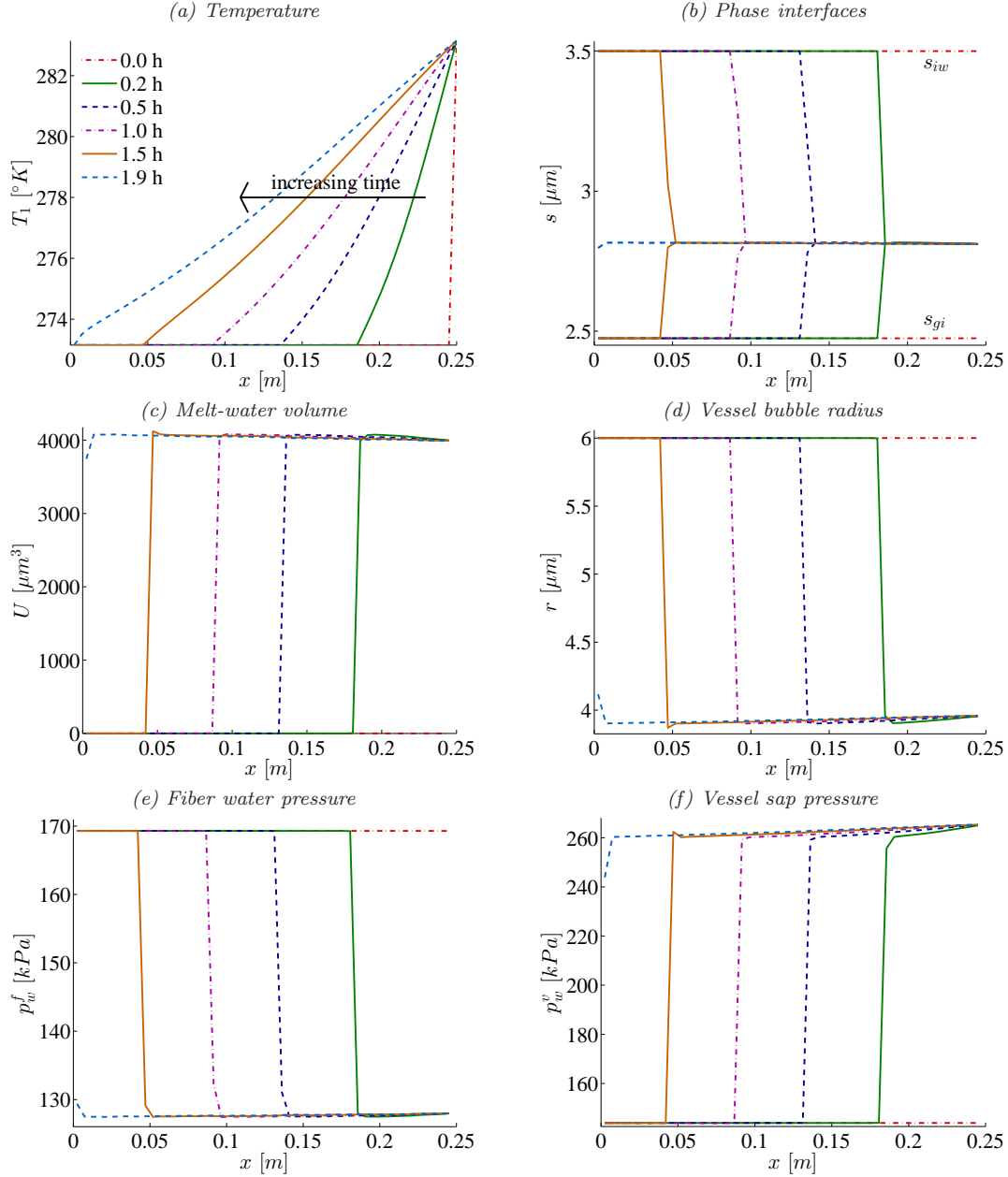


FIGURE 6. Sap exudation simulations showing the solution profiles at a sequence of time points. In all cases, the profiles evolve from right to left as indicated by the arrow in (a).

problem in Section 3.1. The temperature equation is semi-discretized in space using linear Lagrange elements on an equally spaced radial grid, and when coupled with (4.1) the resulting system of ODEs is integrated in time using the Matlab solver `ode15s`. In the second step, the macroscale equation (2.13) is discretized similarly and the global temperature is updated using values of the microscale variables just computed.

After applying the method just described along with the initial and boundary conditions stated earlier, the resulting solutions for  $T_1$ ,  $s_{iw}$  and  $s_{gi}$ ,  $r$ ,  $U$ ,  $p_w^f$  and  $p_w^v$  are illustrated in Figure 6 at a sequence of six times between 0 and 2 h. In each plot, the horizontal ( $x$ ) axis measures radial distance from the center of the tree cross-section. From these plots, it is clear that the solution dynamics for all variables appear as a *melting front* that progresses through the tree from outside to inside (from right to left in the plots) as

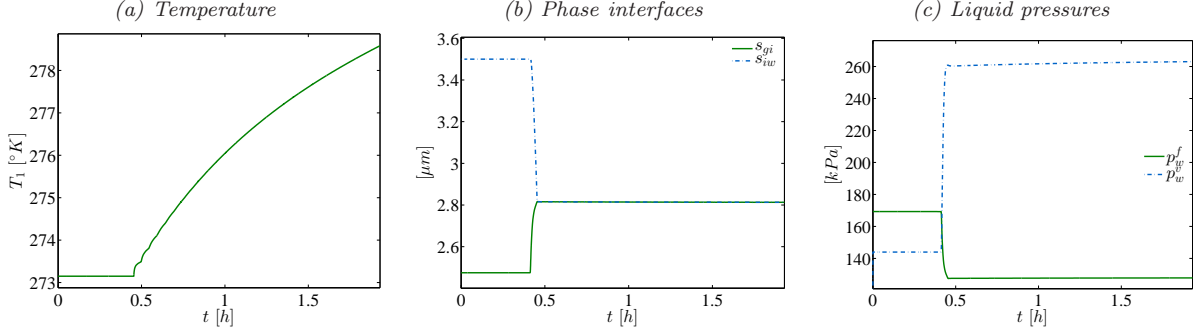


FIGURE 7. Sap exudation simulations, showing the time evolution of various solution components at radial position  $x = 0.15$  m.

the warm ambient air gradually heats up the interior of the tree. Furthermore, the time scale for complete melting of the ice contained in the fibers is just under 2 h.

The temperature profiles vary smoothly in space while other solution quantities are characterized by a steep front that propagates toward the centre of the tree at a speed that decreases with time. The steepness of the melting front derives from the rapid thawing of ice and subsequent adjustment of sap between vessels and fibers on the microscale, all of which occurs during the instant after the temperature exceeds the melting point  $T_c$  at any given location. The reason for the gradual slowing of the melting front with time is that the heat flux naturally decreases the closer the front is to the center of the tree, which in turn leads to a speed decrease owing to the Stefan condition.

There exists a wide separation in the time scales between the slow evolution of the global temperature and the relatively rapid local phase change and sap redistribution, which is clear from the plots in Figure 7 that show the time variation of the solution at radial location  $x = 0.15$  m. These plots are consistent qualitatively with results from simulations of the microscale sap thawing model presented in [5]. We observe that the thickness of the fiber ice layer, which corresponds to the vertical distance between the  $s_{iw}$  and  $s_{gi}$  curves in Figure 7(b), rapidly drops to zero as the ice melts. At the same time, melt-water is driven from fiber to vessel by the pressure stored in the fiber gas bubble, and the pressure plot in Figure 7(c) clearly illustrates the subsequent increase in  $p_w^v$  that we attribute to exudation pressure. After the melting process is complete, the vessel water pressure continues to increase (at a much slower rate not easily visible to the naked eye) owing to further increases in temperature and consequent expansion of the gas in both fiber and vessel.

Upon more careful inspection of the gas/ice and ice/water interface plots in Figure 7(b), we observe that there is a slight time delay in the motion of  $s_{iw}$  relative to  $s_{gi}$ . Indeed, the ice begins to melt at the gas/ice interface (leading to an increase in  $s_{gi}$ ) at a time roughly 25 s in advance of when  $s_{wi}$  starts to drop, which is when a water layer appears between the ice and fiber wall. This phenomenon can be explained as follows. When melt-water first appears in a particular fiber, the gas bubble pressure is so high that water is immediately forced out into the vessel, leaving the ice layer in contact with the fiber wall. The gas pressure then declines until approximately 25 s elapses, at which time the rate of water melting exceeds that of the porous outflow and a water layer begins to accumulate along the fiber wall. By this time, roughly half of the water volume contained in the fiber has been transferred into the vessel.

One of the most important outputs of our sap exudation model is the prediction that the vessel water pressure increases by roughly 120 kPa to a value of  $p_w^v = 263$  kPa. This is related to the exudation pressure if we were able to incorporate freezing effects and simulate the tree over several freeze/thaw cycles. It would therefore be most interesting to compare this pressure increase to experimental measurements of maple trees during the sap harvest season.

Finally, we draw a comparison between results from the sap exudation problem for temperature  $T_1$  and ice layer thickness  $s_{iw} - s_{gi}$ , and the corresponding solutions we obtained for the reduced problem in Section 2. Although the shape of the temperature and ice interface profiles are similar, there is a significant difference in that the melting process for the reduced problem takes over 10 times longer than for the sap exudation problem even though the macroscopic domain and outer temperature are the same. This discrepancy may seem at first to be surprisingly large, but can be attributed to two causes. First of all, the volume of ice to

be melted is more than twice as large in the reduced model since the fibers in the sap exudation problem contain only an annular ring of ice and not a solid circle. Secondly, the diffusion coefficient for the sap exudation problem is roughly 10 times higher because of the much larger value of thermal diffusivity ( $k/\rho c$ ) in the gas phase (with an upper bound of  $2 \times 10^{-5} \text{ m}^2/\text{s}$  based on atmospheric conditions) compared with the corresponding values for ice and water ( $1.2 \times 10^{-6}$  and  $1.3 \times 10^{-7} \text{ m}^2/\text{s}$  respectively) which are the only phases appearing in the reduced model.

**5. Conclusions.** Our aim in this paper was two-fold: first to apply the techniques of periodic homogenization to a two-phase flow problem involving a regular array of melting ice bars that we called the “reduced model”; and second to apply the homogenized equations to study a much more complex three-phase flow problem arising in the context of tree sap exudation. The reduced model is an example of a well-known Stefan problem, and we prove results on existence, uniqueness and a priori estimates for the weak form of the governing equations, which we then use to derive a strong form of the homogenized limit problem. The approach we employ here has the advantage that it applies homogenization techniques in a straightforward manner in order to obtain an uncomplicated limit model, that in turn leads naturally to a simple numerical scheme. Additionally, we are able to encapsulate all microscale processes specific to the maple sap application within the domain  $Y^2$ , wherein the temperature diffuses slowly. We propose a numerical algorithm that captures heat transport on the macroscale, while also incorporating the phase change dynamics taking place on the microscale by solving a corresponding reference cell problem at each point in the domain.

These homogenization equations are then applied to the study of maple sap exudation, which is complicated by a number of extra physical effects including the existence of a gas phase, osmotic pressure, and porous flow between sapwood compartments. The primary novelty in this paper (relative to other work on homogenization of Stefan-type problems) derives from our directly imposing the Dirichlet condition on temperature at the phase interface, which gives rise to a decomposition into fast/slow variables on the sub-regions  $Y^1$  and  $Y^2$ . The major advantage of this approach is that the homogenized equations for the macroscale temperature in the simpler reduced model apply equally well to the sap exudation problem, whereas all remaining physical effects are restricted to the reference cell problem in  $Y^2$ . Moreover, this decomposition leads immediately to a simple and efficient numerical method that we demonstrate is capable of reproducing physically realistic sap exudation pressures.

There are several natural possibilities for future work that arise from this study. In terms of gaining a complete understanding of the sap exudation problem, it is essential to generalize the model to handle the freezing half of the Milburn-O’Malley process, and then to simulate a sequence of daily freeze/thaw cycles. Only then will we be able to see whether this process is capable of capturing the gradual build-up of exudation pressure that is observed in experiments over a period of several days [2]. As part of this work, we will also incorporate the effect of freezing point depression, implement a Robin boundary condition on the tree circumference, and include the dynamics of gas dissolution and nucleation.

It would also be interesting to consider the extension of our analytical results in Section 2 to handle the Robin type boundary condition mentioned above. This has been already done for an unrelated application from T-cell signalling [11], and the extension is straightforward but technically difficult. The Robin condition introduces an extra boundary term in equation (2.2a) through the integration by parts process, which in turn requires an additional one-dimensional homogenization step along the boundary of the domain.

**Appendices.** The following appendices contain proofs of the lemmas and theorems introduced in Section 2. Throughout, we use  $C$  or  $C_i$  to refer to a generic, real, positive constant whose value may change from line to line.

#### Appendix A. Proofs of existence results.

We begin by stating and proving a Lemma A.1 that is not mentioned earlier in this paper but is required in the proof of Lemma 2.2.

**LEMMA A.1.** *Let  $\nabla v \cdot \mathbf{n} \in \mathcal{H}^{-\frac{1}{2}}(\Gamma_\varepsilon)$  for a function  $v \in \mathcal{H}^1(\Omega_\varepsilon)$ . Then there exists a constant  $C > 0$  independent of  $\varepsilon$  such that*

$$\varepsilon \|\varepsilon \nabla v \cdot \mathbf{n}\|_{\mathcal{H}^{-\frac{1}{2}}(\Gamma_\varepsilon)}^2 \leq C \left( \|v\|_{L^2(\Omega_\varepsilon)}^2 + \|\varepsilon \nabla v\|_{L^2(\Omega_\varepsilon)}^2 \right).$$

*Proof.* First we observe that for functions  $v \in \mathcal{H}^1(Y)$ , the Neumann trace mapping [16] guarantees that

$$\|\nabla v \cdot \mathbf{n}\|_{\mathcal{H}^{-\frac{1}{2}}(\Gamma)} \leq C (\|u\|_{L^2(Y)} + \|\nabla v\|_{L^2(Y)})$$

for a constant  $C > 0$ . Next, let  $w \in L^2(\Gamma_\varepsilon)$  and  $\varphi \in \mathcal{H}^{\frac{1}{2}}(\Gamma_\varepsilon)$  and use the fact that  $\mathcal{H}^{\frac{1}{2}} \subset L^2 \subset \mathcal{H}^{-\frac{1}{2}}$  is a Gelfand triple to obtain

$$\begin{aligned} \langle w, \varphi \rangle_{\mathcal{H}^{-\frac{1}{2}}(\Gamma_\varepsilon) \times \mathcal{H}^{\frac{1}{2}}(\Gamma_\varepsilon)} &= (w, \varphi)_{L^2(\Gamma_\varepsilon)} = \int_{\Gamma_\varepsilon} w \varphi \, d\sigma_x = \sum_{k \in K_\varepsilon} \int_{\varepsilon \Gamma} w(x) \varphi(x) \, d\sigma_x \\ &= \sum_{k \in K_\varepsilon} \varepsilon^{n-1} \int_{\Gamma} w(y) \varphi(y) \, d\sigma_y \\ &= \sum_{k \in K_\varepsilon} \varepsilon^{n-1} \langle w, \varphi \rangle_{\mathcal{H}^{-\frac{1}{2}}(\Gamma) \times \mathcal{H}^{\frac{1}{2}}(\Gamma)}, \end{aligned}$$

where  $K_\varepsilon$  refers to the cells of size  $\varepsilon$  in  $\Omega_\varepsilon$  and  $y = \frac{x}{\varepsilon}$ . Since  $L^2(\Gamma_\varepsilon)$  is dense in  $\mathcal{H}^{-\frac{1}{2}}(\Gamma_\varepsilon)$ , the identity also holds for  $v \in \mathcal{H}^{-\frac{1}{2}}(\Gamma_\varepsilon)$  so that

$$\langle v, \varphi \rangle_{\mathcal{H}^{-\frac{1}{2}}(\Gamma_\varepsilon) \times \mathcal{H}^{\frac{1}{2}}(\Gamma_\varepsilon)} = \sum_{k \in K_\varepsilon} \varepsilon^{n-1} \langle v, \varphi \rangle_{\mathcal{H}^{-\frac{1}{2}}(\Gamma) \times \mathcal{H}^{\frac{1}{2}}(\Gamma)}.$$

We can then show that for any  $\varphi \in \mathcal{H}^{\frac{1}{2}}(\Gamma_\varepsilon)$ ,

$$\begin{aligned} \|\varphi\|_{\mathcal{H}^{\frac{1}{2}}(\Gamma_\varepsilon)}^2 &= \int_{\Gamma_\varepsilon} \varphi(x) \, d\sigma_x + \int_{\Gamma_\varepsilon} \int_{\Gamma_\varepsilon} \frac{|\varphi(x_1) - \varphi(x_2)|^2}{|x_1 - x_2|^n} \, d\sigma_{x_1} \, d\sigma_{x_2} \\ &= \sum_{k \in K_\varepsilon} \varepsilon^{n-1} \int_{\Gamma} \varphi(y) \, d\sigma_y + \varepsilon^{2n-2} \int_{\Gamma} \int_{\Gamma} \frac{|\varphi(y_1) - \varphi(y_2)|^2}{|y_1 - y_2|^n} \, d\sigma_{y_1} \, d\sigma_{y_2} \\ &= \varepsilon^{n-1} \|\varphi\|_{L^2(\Gamma)}^2 + \varepsilon^{2n-2} \|\varphi\|_{\mathcal{H}^{\frac{1}{2}}(\Gamma)}^2. \end{aligned}$$

Finally, we come to the main step of the proof in which we estimate

$$\begin{aligned} \|\varepsilon \nabla_x v \cdot \mathbf{n}\|_{\mathcal{H}^{-\frac{1}{2}}(\Gamma_\varepsilon)} &= \sup_{\varphi \neq 0} \frac{\langle \varepsilon \nabla_x v(x) \cdot \mathbf{n}, \varphi(x) \rangle_{\mathcal{H}^{-\frac{1}{2}}(\Gamma_\varepsilon) \times \mathcal{H}^{\frac{1}{2}}(\Gamma_\varepsilon)}}{\|\varphi\|_{\mathcal{H}^{\frac{1}{2}}(\Gamma_\varepsilon)}} \\ &= \sup_{\varphi \neq 0} \sum_{k \in K_\varepsilon} \frac{\varepsilon^{n-1} \langle \nabla_y v(y) \cdot \mathbf{n}, \varphi(y) \rangle_{\mathcal{H}^{-\frac{1}{2}}(\Gamma) \times \mathcal{H}^{\frac{1}{2}}(\Gamma)}}{\varepsilon^{\frac{1}{2}(n-1)} \|\varphi\|_{\mathcal{H}^{\frac{1}{2}}(\Gamma)} + \varepsilon^{n-1} |\varphi|_{\mathcal{H}^{\frac{1}{2}}(\Gamma)}} \\ &= \sup_{\varphi \neq 0} \sum_{k \in K_\varepsilon} \frac{\varepsilon^{n-1} \|\nabla_y v \cdot \mathbf{n}\|_{\mathcal{H}^{-\frac{1}{2}}(\Gamma)} \|\varphi\|_{\mathcal{H}^{\frac{1}{2}}(\Gamma)}}{\varepsilon^{\frac{1}{2}(n-1)} \|\varphi\|_{\mathcal{H}^{\frac{1}{2}}(\Gamma)} + \varepsilon^{n-1} |\varphi|_{\mathcal{H}^{\frac{1}{2}}(\Gamma)}} \\ &\leq \sup_{\varphi \neq 0} \sum_{k \in K_\varepsilon} \frac{C \|v\|_{L^2(Y)} + C \|\nabla_y v\|_{L^2(Y)}}{\varepsilon^{\frac{1}{2}(1-n)} + \frac{|\varphi|_{\mathcal{H}^{\frac{1}{2}}(\Gamma)}}{\|\varphi\|_{\mathcal{H}^{\frac{1}{2}}(\Gamma)}}} \\ &\leq \frac{\sum_{k \in K_\varepsilon} C \left( \sqrt{\int_{\varepsilon Y} v^2 \frac{dx}{\varepsilon^n}} + \sqrt{\int_{\varepsilon Y} \varepsilon^2 |\nabla_x v|^2 \frac{dx}{\varepsilon^n}} \right)}{\varepsilon^{\frac{1}{2}(1-n)} + C_1} \\ &= \frac{\varepsilon^{-\frac{1}{2}n} C (\|v\|_{L^2(\Omega_\varepsilon)} + \|\varepsilon \nabla_x v\|_{L^2(\Omega_\varepsilon)})}{\varepsilon^{\frac{1}{2}(1-n)} + C_1} \\ &\leq \varepsilon^{-\frac{1}{2}} C (\|v\|_{L^2(\Omega_\varepsilon)} + \|\varepsilon \nabla_x v\|_{L^2(\Omega_\varepsilon)}). \end{aligned}$$

Squaring both sides of the inequality yields the desired result.  $\square$

LEMMA 2.2. *The operator  $\mathcal{A} : V \rightarrow V'$  is*

- a) continuous,
- b) bounded, and
- c) coercive, in the sense that there are real constants  $\lambda, \alpha > 0$  such that

$$\mathcal{A}(t, v)(v) + \lambda \|v\|_H^2 \geq \alpha \|v\|_V^2$$

for almost every  $v \in V$  and  $t \in [0, t_m]$ .

*Proof.*

- a) To prove continuity we take any  $\tilde{\varepsilon} > 0$ , require that  $\|u - \tilde{u}\|_V < \delta$  for some  $\delta > 0$ , and then show how to find  $\delta$  so that  $\|\mathcal{A}u - \mathcal{A}\tilde{u}\|_{V'} < \tilde{\varepsilon}$ . We show that for every  $v \in V$  with  $\|v\|_V \leq 1$ ,

$$\begin{aligned} (\mathcal{A}u - \mathcal{A}\tilde{u})v &= (D(u_1)\omega'(u_1)\nabla u_1 - D(\tilde{u}_1)\omega'(\tilde{u}_1)\nabla \tilde{u}_1, \nabla v_1)_{L^2(\Omega_\varepsilon^1)} \\ &\quad + \varepsilon^2 \langle D(u_2)\omega'(u_2)\nabla u_2 - D(\tilde{u}_2)\omega'(\tilde{u}_2)\nabla \tilde{u}_2, v_1 \rangle_{\mathcal{H}^{-\frac{1}{2}}(\Gamma_\varepsilon) \times \mathcal{H}^{\frac{1}{2}}(\Gamma_\varepsilon)} \\ &\quad + \varepsilon^2 (D(u_2)\omega'(u_2)\nabla u_2 - D(\tilde{u}_2)\omega'(\tilde{u}_2)\nabla \tilde{u}_2, \nabla v_2)_{L^2(\Omega_\varepsilon^2)} \\ &\leq \|D(u_1)\omega'(u_1) - D(\tilde{u}_1)\omega'(\tilde{u}_1)\|_{L^\infty(\Omega_\varepsilon^1)} \|\nabla u_1\|_{L^2(\Omega_\varepsilon^1)} \|\nabla v_1\|_{L^2(\Omega_\varepsilon^1)} \\ &\quad + \|D(\tilde{u}_1)\omega'(\tilde{u}_1)\|_{L^\infty(\Omega_\varepsilon^1)} \|\nabla u_1 - \nabla \tilde{u}_1\|_{L^2(\Omega_\varepsilon^1)} \|\nabla v_1\|_{L^2(\Omega_\varepsilon^1)} \\ &\quad + \varepsilon^2 \|D(u_2)\omega'(u_2) - D(\tilde{u}_2)\omega'(\tilde{u}_2)\|_{L^\infty(\Gamma_\varepsilon)} \|\nabla u_2 \cdot \mathbf{n}\|_{\mathcal{H}^{-\frac{1}{2}}(\Gamma_\varepsilon)} \|v_1\|_{\mathcal{H}^{\frac{1}{2}}(\Gamma_\varepsilon)} \\ &\quad + \varepsilon^2 \|D(\tilde{u}_2)\omega'(\tilde{u}_2)\|_{L^\infty(\Gamma_\varepsilon)} \|\nabla u_2 \cdot \mathbf{n} - \nabla \tilde{u}_2 \cdot \mathbf{n}\|_{\mathcal{H}^{-\frac{1}{2}}(\Gamma_\varepsilon)} \|v_1\|_{\mathcal{H}^{\frac{1}{2}}(\Gamma_\varepsilon)} \\ &\quad + \varepsilon^2 \|D(u_2)\omega'(u_2) - D(\tilde{u}_2)\omega'(\tilde{u}_2)\|_{L^\infty(\Omega_\varepsilon^2)} \|\nabla u_2\|_{L^2(\Omega_\varepsilon^2)} \|\nabla v_2\|_{L^2(\Omega_\varepsilon^2)} \\ &\quad + \varepsilon^2 \|D(\tilde{u}_2)\omega'(\tilde{u}_2)\|_{L^\infty(\Omega_\varepsilon^2)} \|\nabla u_2 - \nabla \tilde{u}_2\|_{L^2(\Omega_\varepsilon^2)} \|\nabla v_2\|_{L^2(\Omega_\varepsilon^2)}. \end{aligned}$$

We next apply the trace inequality  $|\Omega_\varepsilon^2| < \infty$  and use the fact that  $\omega'$  and  $D$  are continuous and bounded to conclude that there exists  $\delta_D \leq \delta$  such that  $\|D(u_i)\omega'(u_i) - D(\tilde{u}_i)\omega'(\tilde{u}_i)\|_{L^\infty(\Omega_\varepsilon^i)} < \delta$  and  $\|D(u_i)\omega'(u_i) - D(\tilde{u}_i)\omega'(\tilde{u}_i)\|_{L^\infty(\Gamma_\varepsilon)} < \delta$  when  $\|u_i - \tilde{u}_i\|_V < \delta_D$ , for  $i = 1, 2$ . We may then make use of the fact that  $\|u_i - \tilde{u}_i\|_V < \delta$  and  $\|v\|_V \leq 1$  to obtain

$$\begin{aligned} (\mathcal{A}u - \mathcal{A}\tilde{u})v &\leq \delta (\|\nabla u_1\|_{L^2(\Omega_\varepsilon^1)} + \|D(\tilde{u}_1)\omega'(\tilde{u}_1)\|_{L^\infty(\Omega_\varepsilon^1)}) \\ &\quad + \varepsilon^2 \|\nabla u_2 \cdot \mathbf{n}\|_{\mathcal{H}^{-\frac{1}{2}}(\Gamma_\varepsilon)} + \varepsilon^2 \|D(\tilde{u}_2)\omega'(\tilde{u}_2)\|_{L^\infty(\Gamma_\varepsilon)} \\ &\quad + \varepsilon^2 \|\nabla u_2\|_{L^2(\Omega_\varepsilon^2)} + \varepsilon^2 \|D(\tilde{u}_2)\omega'(\tilde{u}_2)\|_{L^\infty(\Omega_\varepsilon^2)} \\ &= \delta \alpha \leq \tilde{\varepsilon}. \end{aligned}$$

The last inequality is true so long as  $\delta < \frac{\tilde{\varepsilon}}{\alpha}$ .

- b) To show that  $\mathcal{A}$  is bounded, we prove that there exists a constant  $C > 0$  such that

$$(A.1) \quad \mathcal{A}u(v) \leq C \|u\|_V \|v\|_V \quad \text{for any } u, v \in V,$$

which we can derive using the follow sequence of estimates:

$$\begin{aligned} \mathcal{A}u(v) &\leq \max\{D\omega'\} \|\nabla u_1\|_{L^2(\Omega_\varepsilon^1)} \|\nabla v_1\|_{L^2(\Omega_\varepsilon^1)} + \varepsilon^2 \max\{D\omega'\} \|\nabla u_2 \cdot \mathbf{n}\|_{\mathcal{H}^{-\frac{1}{2}}(\Gamma_\varepsilon)} \|v_1\|_{\mathcal{H}^{\frac{1}{2}}(\Gamma_\varepsilon)} \\ &\quad + \varepsilon^2 \max\{D\omega'\} \|\nabla u_2\|_{L^2(\Omega_\varepsilon^2)} \|\nabla v_2\|_{L^2(\Omega_\varepsilon^2)} \\ &\leq \max\{D\omega'\} \|\nabla u_1\|_{L^2(\Omega_\varepsilon^1)} \|\nabla v_1\|_{L^2(\Omega_\varepsilon^1)} + \varepsilon^2 \max\{D\omega'\} \|\nabla u_2\|_{L^2(\Omega_\varepsilon^2)} \|\nabla v_2\|_{L^2(\Omega_\varepsilon^2)} \\ &\quad + \max\{D\omega'\} c_0 (\|u_2\|_{L^2(\Omega_\varepsilon^2)} + \|\varepsilon \nabla u_2\|_{L^2(\Omega_\varepsilon^2)}) (\|v_1\|_{L^2(\Omega_\varepsilon^1)} + \|\varepsilon \nabla v_1\|_{L^2(\Omega_\varepsilon^1)}) \\ &\leq (\max\{D\omega'\} + c_0 \max\{D\omega'\} + \varepsilon^2 \max\{D\omega'\}) \|u\|_V \|v\|_V. \end{aligned}$$

Hence, the operator  $\mathcal{A}$  is bounded as in (A.1) for every  $0 < \varepsilon < 1$  with the constant

$$C = \max\{D\omega'\} + c_0 \max\{D\omega'\} + \max\{D\omega'\}.$$

c) For coercivity we proceed by deriving the following estimates for

$$\begin{aligned}
\mathcal{A}v(v) + \lambda \|v\|_H^2 &= (D(v_1)\omega'(v_1)\nabla v_1, \nabla v_1)_{\Omega_\varepsilon^1} + \langle \varepsilon^2 D(v_2)\omega'(v_2)\nabla v_2 \cdot \mathbf{n}, v_1 \rangle_{\mathcal{H}^{-\frac{1}{2}}(\Gamma_\varepsilon) \times \mathcal{H}^{\frac{1}{2}}(\Gamma_\varepsilon)} \\
&\quad + (\varepsilon^2 D(v_2)\omega'(v_2)\nabla v_2, \nabla v_2)_{\Omega_\varepsilon^2} + \lambda \|v_1\|_{\Omega_\varepsilon^1}^2 + \lambda \|v_2\|_{\Omega_\varepsilon^2}^2 \\
&\geq \min\{D\omega'\} \|\nabla v_1\|_{\Omega_\varepsilon^1}^2 - \max\{D\omega'\} c_0 \left( \|v_2\|_{\Omega_\varepsilon^2}^2 + \varepsilon^2 \|\nabla v_2\|_{\Omega_\varepsilon^2}^2 + \|v_1\|_{\Omega_\varepsilon^1}^2 + \varepsilon^2 \|\nabla v_1\|_{\Omega_\varepsilon^1}^2 \right) \\
&\quad + \min\{D\omega'\} \varepsilon^2 \|\nabla v_2\|_{\Omega_\varepsilon^2}^2 + \lambda \|v_1\|_{\Omega_\varepsilon^1}^2 + \lambda \|v_2\|_{\Omega_\varepsilon^2}^2 \\
&\geq \|v_1\|_{\Omega_\varepsilon^1}^2 (\lambda - \max\{D\omega'\} c_0) + \|\nabla v_1\|_{\Omega_\varepsilon^1}^2 (\min\{D\omega'\} - \max\{D\omega'\} c_0 \varepsilon^2) \\
&\quad + \|v_2\|_{\Omega_\varepsilon^2}^2 (\lambda - \max\{D\omega'\} c_0) + \|\nabla v_2\|_{\Omega_\varepsilon^2}^2 \varepsilon^2 (\min\{D\omega'\} - \max\{D\omega'\} c_0) \\
&\geq \alpha \|v\|_V^2,
\end{aligned}$$

as required. We have merged all constants from the second-to-last expression into a single constant  $\alpha > 0$ , which is possible provided that  $(\min\{D\omega'\} - \max\{D\omega'\} c_0) > 0$ , and after choosing both  $\varepsilon$  small enough and  $\lambda$  big enough. We also applied Lemma A.1 in the derivation of the second inequality above.  $\square$

## Appendix B. Proofs of results related to a priori estimates.

LEMMA 2.3. *Here,  $C$  or  $C_i$  represents a positive constant that is independent of  $\varepsilon$ .*

a) *There exists a constant  $C_1$  such that*

$$\|T_{1,\varepsilon}\|_{\Omega_\varepsilon^1}^2 + \|\nabla T_{1,\varepsilon}\|_{\Omega_\varepsilon^1}^2 + \|T_{2,\varepsilon}\|_{\Omega_\varepsilon^2}^2 + \varepsilon^2 \|\nabla T_{2,\varepsilon}\|_{\Omega_\varepsilon^2}^2 \leq C_1.$$

b) *There exists a constant  $C_2$  such that*

$$\|\nabla E_{1,\varepsilon}\|_{\Omega_\varepsilon^1}^2 + \|\nabla \cdot [D(E_{1,\varepsilon})\nabla T_{1,\varepsilon}]\|_{\Omega_\varepsilon^1,t}^2 + \varepsilon^2 \|\nabla E_{2,\varepsilon}\|_{\Omega_\varepsilon^2}^2 + \varepsilon^4 \|\nabla \cdot [D(E_{2,\varepsilon})\nabla T_{2,\varepsilon}]\|_{\Omega_\varepsilon^2,t}^2 \leq C_2.$$

c) *There exists a constant  $C_3$  such that*

$$\varepsilon^3 \|D(E_{2,\varepsilon})\nabla T_{2,\varepsilon}\|_{\Gamma_\varepsilon,t}^2 \leq C_3.$$

d) *The functions  $E_{1,\varepsilon}$ ,  $E_{2,\varepsilon}$  are nonnegative for almost every  $x \in \Omega_\varepsilon^1$ ,  $\Omega_\varepsilon^2$  as long as  $E_{1,\varepsilon}(0)$ ,  $E_{2,\varepsilon}(0)$  are nonnegative (respectively).*

e) *There exists a constant  $C_4$  such that*

$$\|E_{1,\varepsilon}\|_{L^\infty(\Omega_\varepsilon^1)} + \|E_{2,\varepsilon}\|_{L^\infty(\Omega_\varepsilon^2)} \leq C_4.$$

f) *There exists a constant  $C_5$  such that*

$$\|\partial_t E_{1,\varepsilon}\|_{L^2([0,t_m],L^2(\Omega_\varepsilon^1))} + \|\partial_t E_{2,\varepsilon}\|_{L^2([0,t_m],L^2(\Omega_\varepsilon^2))} \leq C_5.$$

*Proof.*

a) We test equation (2.2) with  $(T_{1,\varepsilon}, T_{2,\varepsilon})$  to obtain

$$\begin{aligned}
(\partial_t E_{1,\varepsilon}, T_{1,\varepsilon})_{\Omega_\varepsilon^1} + (D(E_{1,\varepsilon})\nabla T_{1,\varepsilon}, \nabla T_{1,\varepsilon})_{\Omega_\varepsilon^1} + \varepsilon^2 \langle D(E_{2,\varepsilon})\nabla T_{2,\varepsilon} \cdot \mathbf{n}, T_{1,\varepsilon} \rangle_{\Gamma_\varepsilon} &= 0, \\
(\partial_t E_{2,\varepsilon}, T_{2,\varepsilon})_{\Omega_\varepsilon^2} + \varepsilon^2 (D(E_{2,\varepsilon})\nabla T_{2,\varepsilon}, \nabla T_{2,\varepsilon})_{\Omega_\varepsilon^2} - \varepsilon^2 \langle D(E_{2,\varepsilon})\nabla T_{2,\varepsilon} \cdot \mathbf{n}, T_{1,\varepsilon} \rangle_{\Gamma_\varepsilon} &= 0,
\end{aligned}$$

where we have the boundary term in the second equation because  $T_{2,\varepsilon} = T_{1,\varepsilon}$  is not zero at  $\Gamma_\varepsilon$ . The two equations may then be added to eliminate the boundary terms, after which we rewrite the enthalpy variables in terms of temperature using chain rule:

$$\begin{aligned}
((\omega^{-1})' \partial_t T_{1,\varepsilon}, T_{1,\varepsilon})_{\Omega_\varepsilon^1} + \min\{D\} (\nabla T_{1,\varepsilon}, \nabla T_{1,\varepsilon})_{\Omega_\varepsilon^1} + ((\omega^{-1})' \partial_t T_{2,\varepsilon}, T_{2,\varepsilon})_{\Omega_\varepsilon^2} \\
+ \varepsilon^2 \min\{D\} (\nabla T_{2,\varepsilon}, \nabla T_{2,\varepsilon})_{\Omega_\varepsilon^2} = 0.
\end{aligned}$$

Next, using that  $(\omega^{-1})'$  and  $D$  are both bounded and positive, we can integrate in time to obtain

$$\begin{aligned} & \frac{1}{2} \min\{(\omega^{-1})'\} \|T_{1,\varepsilon}\|_{\Omega_\varepsilon^1}^2 + \min\{D\} \|\nabla T_{1,\varepsilon}\|_{\Omega_\varepsilon^1,t}^2 + \frac{1}{2} \min\{(\omega^{-1})'\} \|T_{2,\varepsilon}\|_{\Omega_\varepsilon^2}^2 + \min\{D\} \|\nabla T_{2,\varepsilon}\|_{\Omega_\varepsilon^2,t}^2 \\ & \leq \frac{1}{2} \max\{(\omega^{-1})'\} \|T_{1,\varepsilon}(0)\|_{\Omega_\varepsilon^1}^2 + \frac{1}{2} \max\{(\omega^{-1})'\} \|T_{2,\varepsilon}(0)\|_{\Omega_\varepsilon^2}^2. \end{aligned}$$

Since the initial conditions are bounded, we obtain by merging the constants that

$$\|T_{1,\varepsilon}\|_{\Omega_\varepsilon^1}^2 + \|\nabla T_{1,\varepsilon}\|_{\Omega_\varepsilon^1}^2 + \|T_{2,\varepsilon}\|_{\Omega_\varepsilon^2}^2 + \varepsilon^2 \|\nabla T_{2,\varepsilon}\|_{\Omega_\varepsilon^2}^2 \leq C_1,$$

for a constant  $C_1 > 0$  that is independent of  $\varepsilon$ . With  $\omega$  and  $\omega^{-1}$  being continuous and bounded, and with  $E_{1,\varepsilon} = \omega^{-1}(T_{1,\varepsilon})$  and  $E_{2,\varepsilon} = \omega^{-1}(T_{2,\varepsilon})$ , it follows that  $\|E_{1,\varepsilon}\|_{\Omega_\varepsilon^1}^2 + \|E_{2,\varepsilon}\|_{\Omega_\varepsilon^2}^2 \leq C_1$ .

- b) We test equation (2.2) with  $(\nabla \cdot [D(E_{1,\varepsilon}) \nabla T_{1,\varepsilon}], \varepsilon^2 \nabla \cdot [D(E_{2,\varepsilon}) \nabla T_{2,\varepsilon}])$ , which can be made rigorous as in Lemma 7.23 of [10]:

$$\begin{aligned} & (\partial_t E_{1,\varepsilon}, \nabla \cdot [D(E_{1,\varepsilon}) \nabla T_{1,\varepsilon}])_{\Omega_\varepsilon^1} - \|\nabla \cdot [D(E_{1,\varepsilon}) \nabla T_{1,\varepsilon}]\|_{\Omega_\varepsilon^1}^2 = 0, \\ & \varepsilon^2 (\partial_t E_{2,\varepsilon}, \nabla \cdot [D(E_{2,\varepsilon}) \nabla T_{2,\varepsilon}])_{\Omega_\varepsilon^2} - \varepsilon^4 \|\nabla \cdot [D(E_{2,\varepsilon}) \nabla T_{2,\varepsilon}]\|_{\Omega_\varepsilon^2}^2 = 0. \end{aligned}$$

Integrating by parts in the first term of each equation yields

$$\begin{aligned} & -(\partial_t \nabla E_{1,\varepsilon}, D(E_{1,\varepsilon}) \nabla T_{1,\varepsilon})_{\Omega_\varepsilon^1} - \varepsilon^2 \langle \partial_t E_{1,\varepsilon}, D(E_{2,\varepsilon}) \nabla T_{2,\varepsilon} \cdot \mathbf{n} \rangle_{\Gamma_\varepsilon} - \|\nabla \cdot [D(E_{1,\varepsilon}) \nabla T_{1,\varepsilon}]\|_{\Omega_\varepsilon^1}^2 = 0, \\ & -\varepsilon^2 (\partial_t \nabla E_{2,\varepsilon}, D(E_{2,\varepsilon}) \nabla T_{2,\varepsilon})_{\Omega_\varepsilon^2} + \varepsilon^2 \langle \partial_t E_{1,\varepsilon}, D(E_{2,\varepsilon}) \nabla T_{2,\varepsilon} \cdot \mathbf{n} \rangle_{\Gamma_\varepsilon} - \varepsilon^4 \|\nabla \cdot [D(E_{2,\varepsilon}) \nabla T_{2,\varepsilon}]\|_{\Omega_\varepsilon^2}^2 = 0, \end{aligned}$$

where we have also applied the boundary conditions on  $\Gamma_\varepsilon$ . Adding the last two equations together and swapping sign yields

$$\begin{aligned} & (\partial_t \nabla E_{1,\varepsilon}, D(E_{1,\varepsilon}) \omega'(E_{1,\varepsilon}) \nabla E_{1,\varepsilon})_{\Omega_\varepsilon^1} + \|\nabla \cdot [D(E_{1,\varepsilon}) \nabla T_{1,\varepsilon}]\|_{\Omega_\varepsilon^1}^2 \\ & + \varepsilon^2 (\partial_t \nabla E_{2,\varepsilon}, D(E_{2,\varepsilon}) \omega'(E_{2,\varepsilon}) \nabla E_{2,\varepsilon})_{\Omega_\varepsilon^2} + \varepsilon^4 \|\nabla \cdot [D(E_{2,\varepsilon}) \nabla T_{2,\varepsilon}]\|_{\Omega_\varepsilon^2}^2 = 0. \end{aligned}$$

We then integrate with respect to time and use the fact that  $\omega'$  and  $D$  are bounded and positive to obtain

$$\begin{aligned} & \frac{1}{2} \min\{D\omega'\} \|\nabla E_{1,\varepsilon}\|_{\Omega_\varepsilon^1}^2 + \|\nabla \cdot [D(E_{1,\varepsilon}) \nabla T_{1,\varepsilon}]\|_{\Omega_\varepsilon^1,t}^2 + \frac{\varepsilon^2}{2} \min\{D\omega'\} \|\nabla E_{2,\varepsilon}\|_{\Omega_\varepsilon^2}^2 + \varepsilon^4 \|\nabla \cdot [D(E_{2,\varepsilon}) \nabla T_{2,\varepsilon}]\|_{\Omega_\varepsilon^2,t}^2 \\ & \leq \frac{1}{2} \max\{D\omega'\} \|\nabla E_{1,\varepsilon}(0)\|_{\Omega_\varepsilon^1}^2 + \frac{\varepsilon^2}{2} \max\{D\omega'\} \|\nabla E_{2,\varepsilon,t}(0)\|_{\Omega_\varepsilon^2}^2 \\ & \leq C, \end{aligned}$$

where we combined the smooth and bounded initial conditions into a single constant  $C$ . Merging all constants into a single  $C_2 > 0$  yields

$$\|\nabla E_{1,\varepsilon}\|_{\Omega_\varepsilon^1}^2 + \|\nabla \cdot [D(E_{1,\varepsilon}) \nabla T_{1,\varepsilon}]\|_{\Omega_\varepsilon^1,t}^2 + \varepsilon^2 \|\nabla E_{2,\varepsilon}\|_{\Omega_\varepsilon^2}^2 + \varepsilon^4 \|\nabla \cdot [D(E_{2,\varepsilon}) \nabla T_{2,\varepsilon}]\|_{\Omega_\varepsilon^2,t}^2 \leq C_2.$$

- c) The proof is a straightforward application of parts a) and b) along with the trace inequality, which yield

$$\varepsilon^3 \|D(E_{2,\varepsilon}) \nabla T_{2,\varepsilon}\|_{\Gamma_\varepsilon,t}^2 \leq \varepsilon^2 \|D(E_{2,\varepsilon}) \nabla T_{2,\varepsilon}\|_{\Omega_\varepsilon^2,t}^2 + \varepsilon^4 \|\nabla \cdot [D(E_{2,\varepsilon}) \nabla T_{2,\varepsilon}]\|_{\Omega_\varepsilon^2,t}^2 \leq C_3.$$

- d) We test equation (2.2) with  $(E_{1,\varepsilon-}, E_{2,\varepsilon-})$ , where  $E_{1,\varepsilon-} = -E_{1,\varepsilon}$  if  $E_{1,\varepsilon} \leq 0$  pointwise and  $E_{1,\varepsilon-} = 0$  otherwise; an analogous definition is used for  $E_{2,\varepsilon-}$ . We then find that

$$\begin{aligned} & (\partial_t E_{1,\varepsilon-}, E_{1,\varepsilon-})_{\Omega_\varepsilon^1} + (D(E_{1,\varepsilon-}) \nabla T_{1,\varepsilon}, \nabla E_{1,\varepsilon-})_{\Omega_\varepsilon^1} + \varepsilon^2 \langle D(E_{2,\varepsilon}) \nabla T_{2,\varepsilon}, E_{1,\varepsilon-} \rangle_{\Gamma_\varepsilon} = 0, \\ & (\partial_t E_{2,\varepsilon-}, E_{2,\varepsilon-})_{\Omega_\varepsilon^2} + \varepsilon^2 (D(E_{2,\varepsilon-}) \nabla T_{2,\varepsilon}, \nabla E_{2,\varepsilon-})_{\Omega_\varepsilon^2} - \varepsilon^2 \langle D(E_{2,\varepsilon}) \nabla T_{2,\varepsilon}, E_{1,\varepsilon-} \rangle_{\Gamma_\varepsilon} = 0, \end{aligned}$$



where we have used that  $E_{2,\varepsilon-} = E_{1,\varepsilon-}$  on  $\Gamma_\varepsilon$ . Add the two equations above, substitute  $T_{2,\varepsilon} = \omega(E_{2,\varepsilon})$  and  $T_{1,\varepsilon} = \omega(E_{1,\varepsilon})$ , and then integrate over the time interval  $[0, t]$  to obtain

$$\frac{1}{2}\|E_{1,\varepsilon-}\|_{\Omega_\varepsilon^1}^2 + \min\{D\omega'\}\|\nabla E_{1,\varepsilon-}\|_{\Omega_\varepsilon^1,t}^2 + \frac{1}{2}\|E_{2,\varepsilon-}\|_{\Omega_\varepsilon^2}^2 + \varepsilon^2 \min\{D\omega'\}\|\nabla E_{2,\varepsilon-}\|_{\Omega_\varepsilon^2,t}^2 \leq 0,$$

where we assumed that the initial conditions are nonnegative. This yields that  $E_{1,\varepsilon}, E_{2,\varepsilon} \geq 0$  almost everywhere, from which we can conclude that  $E_{1,\varepsilon}, E_{2,\varepsilon}$  are bounded from below in  $L^2([0, t_m], L^\infty(\Omega_\varepsilon^2))$ , independently of  $\varepsilon$ .

- e) Let  $M(t) = \max\{\|E_{1,\varepsilon}(0)\|_{L^\infty(\Omega_\varepsilon^1)}, \|E_{2,\varepsilon}(0)\|_{L^\infty(\Omega_\varepsilon^2)}\}e^{kt}$  for some constant  $k \in \mathbb{R}$ . We test equation (2.2) with  $((E_{1,\varepsilon} - M)_+, (E_{2,\varepsilon} - M)_+)$ , where  $(E_{1,\varepsilon} - M)_+ = E_{1,\varepsilon} - M$  if  $E_{1,\varepsilon} \leq M$  pointwise and  $(E_{1,\varepsilon} - M)_+ = 0$  otherwise; an analogous definition is used for  $(E_{2,\varepsilon} - M)_+$ . We then obtain that

$$\begin{aligned} &(\partial_t E_{1,\varepsilon}, (E_{1,\varepsilon} - M)_+)_{\Omega_\varepsilon^1} + (D(E_{1,\varepsilon})\nabla T_{1,\varepsilon}, \nabla(E_{1,\varepsilon} - M)_+)_{\Omega_\varepsilon^1} + \varepsilon^2 \langle D(E_{2,\varepsilon})\nabla T_{2,\varepsilon}, (E_{1,\varepsilon} - M)_+ \rangle_{\Gamma_\varepsilon} = 0, \\ &(\partial_t E_{2,\varepsilon}, (E_{2,\varepsilon} - M)_+)_{\Omega_\varepsilon^2} + \varepsilon^2 (D(E_{2,\varepsilon})\nabla T_{2,\varepsilon}, \nabla(E_{2,\varepsilon} - M)_+)_{\Omega_\varepsilon^2} - \varepsilon^2 \langle D(E_{2,\varepsilon})\nabla T_{2,\varepsilon}, (E_{1,\varepsilon} - M)_+ \rangle_{\Gamma_\varepsilon} = 0, \end{aligned}$$

where  $(E_{1,\varepsilon} - M)_+ = (E_{2,\varepsilon} - M)_+$  on  $\Gamma_\varepsilon$ . Next, we subtract  $\partial_t M = kM$  from the first inner product term in both equations and the corresponding term from the right-hand side. Then both equations are added together so that the boundary-term cancels, leaving

$$\begin{aligned} &(\partial_t(E_{1,\varepsilon} - M)_+, (E_{1,\varepsilon} - M)_+)_{\Omega_\varepsilon^1} + (D(E_{1,\varepsilon})\omega'(E_{1,\varepsilon})\nabla E_{1,\varepsilon}, \nabla(E_{1,\varepsilon} - M)_+)_{\Omega_\varepsilon^1} \\ &+ (\partial_t(E_{2,\varepsilon} - M)_+, (E_{2,\varepsilon} - M)_+)_{\Omega_\varepsilon^2} + \varepsilon^2 (D(E_{2,\varepsilon})\omega'(E_{2,\varepsilon})\nabla E_{2,\varepsilon}, \nabla(E_{2,\varepsilon} - M)_+)_{\Omega_\varepsilon^2} \\ &= (-kM, (E_{1,\varepsilon} - M)_+)_{\Omega_\varepsilon^1} + (-kM, (E_{2,\varepsilon} - M)_+)_{\Omega_\varepsilon^2}. \end{aligned}$$

Because  $\nabla M = 0$ , we may subtract  $\nabla M$  from the second term, while at the same time estimating  $D\omega'$  to obtain

$$\begin{aligned} &(\partial_t(E_{1,\varepsilon} - M)_+, (E_{1,\varepsilon} - M)_+)_{\Omega_\varepsilon^1} + \min\{D\omega'\}(\nabla(E_{1,\varepsilon} - M), \nabla(E_{1,\varepsilon} - M)_+)_{\Omega_\varepsilon^1} \\ &+ (\partial_t(E_{2,\varepsilon} - M)_+, (E_{2,\varepsilon} - M)_+)_{\Omega_\varepsilon^2} + \varepsilon^2 \min\{D\omega'\}(\nabla(E_{2,\varepsilon} - M), \nabla(E_{2,\varepsilon} - M)_+)_{\Omega_\varepsilon^2} \\ &= (-kM, (E_{1,\varepsilon} - M)_+)_{\Omega_\varepsilon^1} + (-kM, (E_{2,\varepsilon} - M)_+)_{\Omega_\varepsilon^2}. \end{aligned}$$

Finally, integrating with respect to time yields

$$\begin{aligned} &\frac{1}{2}\|(E_{1,\varepsilon} - M)_+\|_{\Omega_\varepsilon^1}^2 + \min\{D\omega'\}\|\nabla(E_{1,\varepsilon} - M)_+\|_{\Omega_\varepsilon^1,t}^2 \\ &+ \frac{1}{2}\|(E_{2,\varepsilon} - M)_+\|_{\Omega_\varepsilon^2}^2 + \varepsilon^2 \min\{D\omega'\}\|\nabla(E_{2,\varepsilon} - M)_+\|_{\Omega_\varepsilon^2,t}^2 \\ &\leq -(kM, (E_{1,\varepsilon} - M)_+)_{\Omega_\varepsilon^1,t} - (kM, (E_{2,\varepsilon} - M)_+)_{\Omega_\varepsilon^2,t} \leq 0, \end{aligned}$$

where we used that the initial conditions are smaller than  $M$ . Hence, we find that  $\|(E_{1,\varepsilon} - M)_+\|_{\Omega_\varepsilon^1}^2 + \|(E_{2,\varepsilon} - M)_+\|_{\Omega_\varepsilon^2}^2 \leq 0$  which means  $E_{1,\varepsilon} \leq M$  and  $E_{2,\varepsilon} \leq M$  almost everywhere.

- f) We consider equations (2.2) before integration by parts

$$\begin{aligned} \partial_t E_{1,\varepsilon} &= \nabla \cdot [D(E_{1,\varepsilon})\nabla T_{1,\varepsilon}] & \text{in } \Omega_\varepsilon^1, \\ \partial_t E_{2,\varepsilon} &= \nabla \cdot [D(E_{2,\varepsilon})\nabla T_{2,\varepsilon}] & \text{in } \Omega_\varepsilon^2, \end{aligned}$$

and apply the  $L^2$ -norm over  $[0, t_m] \times \Omega_\varepsilon^1$  and  $[0, t_m] \times \Omega_\varepsilon^2$ , respectively. Then we can use item b) of this Lemma to obtain

$$\begin{aligned} \|\partial_t E_{1,\varepsilon}\|_{\Omega_\varepsilon^1,t} &= \|\nabla \cdot [D(E_{1,\varepsilon})\nabla T_{1,\varepsilon}]\|_{\Omega_\varepsilon^1,t} \leq C_5, \\ \|\partial_t E_{2,\varepsilon}\|_{\Omega_\varepsilon^2,t} &= \|\nabla \cdot [D(E_{2,\varepsilon})\nabla T_{2,\varepsilon}]\|_{\Omega_\varepsilon^2,t} \leq C_5, \end{aligned}$$

where constant  $C_5$  is independent of  $\varepsilon$ .

□

### Appendix C. Proof of uniqueness.

THEOREM 2.4. *Equations (2.12) have at most one solution given by*

$$\begin{aligned} T_1 \in \mathcal{V}^1(\Omega) + T_a &= L^2([0, t_m], \mathcal{H}_0^1(\Omega)) \cap \mathcal{H}^1([0, t_m], L^2(\Omega)) + T_a, \\ T_2 \in \mathcal{V}^2(\Omega \times Y^2) + T_1 &= L^2([0, t_m], L^2(\Omega, \mathcal{H}_\#^1(Y^2))) \cap \mathcal{H}^1([0, t_m], L^2(\Omega \times Y^2)) + T_1, \end{aligned}$$

where  $T_1 = \omega(E_1)$  and  $T_2 = \omega(E_2)$ .

*Proof.* First, we note that the cell problem (2.9) has a unique solution, which is proven in [13]. Hence, we will only prove uniqueness of the macroscopic problem by assuming that there are two solutions  $(E_{1,a}, T_{1,a}, E_{2,a}, T_{2,a})$  and  $(E_{1,b}, T_{1,b}, E_{2,b}, T_{2,b})$ , and then showing that they are equal. We start by substituting our two solutions into the second equation of (2.12), subtracting, and then testing with the functions  $E_{1,a} - E_{1,b}$  and  $E_{2,a} - E_{2,b}$ :

$$\begin{aligned} |Y^1|(\partial_t E_{1,a} - \partial_t E_{1,b}, E_{1,a} - E_{1,b})_\Omega + \Pi(D(E_{1,a})\nabla T_{1,a} - D(E_{1,b})\nabla T_{1,b}, \nabla E_{1,a} - \nabla E_{1,b})_\Omega \\ + (D(E_{2,a})\nabla T_{2,a} \cdot \mathbf{n} - D(E_{2,b})\nabla T_{2,b} \cdot \mathbf{n}, E_{1,a} - E_{1,b})_{\Omega \times \Gamma} = 0, \\ (\partial_t E_{2,a} - \partial_t E_{2,b}, E_{2,a} - E_{2,b})_{\Omega \times Y^2} + (D_2(E_{2,a})\nabla_y T_{2,a} - D_2(E_{2,b})\nabla_y T_{2,b}, \nabla_y E_{2,a} - \nabla_y E_{2,b})_{\Omega \times Y^2} \\ - (D(E_{2,a})\nabla T_{2,a} \cdot \mathbf{n} - D(E_{2,b})\nabla T_{2,b} \cdot \mathbf{n}, E_{1,a} - E_{1,b})_{\Omega \times \Gamma} = 0. \end{aligned}$$

Adding these two equations, using  $T = \omega(E)$ , and adding/subtracting an extra term we obtain

$$\begin{aligned} |Y^1|(\partial_t E_{1,a} - \partial_t E_{1,b}, E_{1,a} - E_{1,b})_\Omega + \Pi(D(E_{1,a})\omega'(E_{1,a})\nabla E_{1,a} - D(E_{1,a})\omega'(E_{1,a})\nabla E_{1,b} \\ + D(E_{1,a})\omega'(E_{1,a})\nabla E_{1,b} - D(E_{1,b})\omega'(E_{1,b})\nabla E_{1,b}, \nabla E_{1,a} - \nabla E_{1,b})_\Omega \\ + (\partial_t E_{2,a} - \partial_t E_{2,b}, E_{2,a} - E_{2,b})_{\Omega \times Y^2} + (D(E_{2,a})\omega'(E_{2,a})\nabla_y E_{2,a} - D(E_{2,a})\omega'(E_{2,a})\nabla_y E_{2,b} \\ + D(E_{2,a})\omega'(E_{2,a})\nabla_y E_{2,b} - D(E_{2,b})\omega'(E_{2,b})\nabla_y E_{2,b}, \nabla_y E_{2,a} - \nabla_y E_{2,b})_{\Omega \times Y^2} = 0. \end{aligned}$$

Then we can develop the following estimate

$$\begin{aligned} |Y^1|(\partial_t E_{1,a} - \partial_t E_{1,b}, E_{1,a} - E_{1,b})_\Omega + \Pi \min\{D\omega'\} \|\nabla E_{1,a} - \nabla E_{1,b}\|_\Omega^2 \\ + (\partial_t E_{2,a} - \partial_t E_{2,b}, E_{2,a} - E_{2,b})_{\Omega \times Y^2} + \min\{D\omega'\} \|\nabla_y E_{2,a} - \nabla_y E_{2,b}\|_{\Omega \times Y^2}^2 \\ = -((D(E_{1,a})\omega'(E_{1,a}) - D(E_{1,b})\omega'(E_{1,b}))\nabla E_{1,b}, \nabla E_{1,a} - \nabla E_{1,b})_\Omega \\ - ((D(E_{2,a})\omega'(E_{2,a}) - D(E_{2,b})\omega'(E_{2,b}))\nabla_y E_{2,b}, \nabla_y E_{2,a} - \nabla_y E_{2,b})_{\Omega \times Y^2} \\ \leq C_D \|(E_{1,a} - E_{1,b})\nabla E_{1,b}\|_\Omega \|\nabla E_{1,a} - \nabla E_{1,b}\|_\Omega \\ + C_D \|(E_{2,a} - E_{2,b})\nabla_y E_{2,b}\|_{\Omega \times Y^2} \|\nabla_y E_{2,a} - \nabla_y E_{2,b}\|_{\Omega \times Y^2}, \end{aligned}$$

where we used that  $D\omega'$  is Lipschitz continuous with constant  $C_D$ . Now we continue applying the quadratic formula and integrating with respect to time

$$\begin{aligned} \frac{1}{2}|Y^1| \|E_{1,a} - E_{1,b}\|_\Omega^2 + \Pi \min\{D\omega'\} \|\nabla E_{1,a} - \nabla E_{1,b}\|_{\Omega,t}^2 \\ + \frac{1}{2} \|E_{2,a} - E_{2,b}\|_{\Omega \times Y^2}^2 + \min\{D\omega'\} \|\nabla_y E_{2,a} - \nabla_y E_{2,b}\|_{\Omega \times Y^2,t}^2 \\ \leq \frac{C_D \lambda}{2} \|(E_{1,a} - E_{1,b})\nabla E_{1,b}\|_{\Omega,t}^2 + \frac{C_D}{2\lambda} \|\nabla E_{1,a} - \nabla E_{1,b}\|_{\Omega,t}^2 \\ + \frac{C_D \lambda}{2} \|(E_{2,a} - E_{2,b})\nabla_y E_{2,b}\|_{\Omega \times Y^2,t}^2 + \frac{1}{2\lambda} C_D \|\nabla_y E_{2,a} - \nabla_y E_{2,b}\|_{\Omega \times Y^2,t}^2, \end{aligned}$$

for any  $\lambda > 0$ , where we have taken advantage of the fact that the initial conditions cancel. Rearranging

terms yields

$$\begin{aligned} & \frac{1}{2} |Y^1| \|E_{1,a} - E_{1,b}\|_{\Omega}^2 + \left( \Pi \min\{D\omega'\} - \frac{C_D}{2\lambda} \right) \|\nabla E_{1,a} - \nabla E_{1,b}\|_{\Omega,t}^2 \\ & \quad + \frac{1}{2} \|E_{2,a} - E_{2,b}\|_{\Omega \times Y^2}^2 + \left( \min\{D\omega'\} - \frac{C_D}{2\lambda} \right) \|\nabla_y E_{2,a} - \nabla E_{2,b}\|_{\Omega \times Y^2,t}^2 \\ & \leq \frac{C_D \lambda}{2} \|(E_{1,a} - E_{1,b}) \nabla E_{1,b}\|_{\Omega,t}^2 + \frac{C_D \lambda}{2} \|(E_{2,a} - E_{2,b}) \nabla_y E_{2,b}\|_{\Omega \times Y^2,t}^2. \end{aligned}$$

Then we choose  $\lambda$  large enough such that on the left-hand side all terms are positive, after which we can apply Gronwall's Lemma to obtain

$$\|E_{1,a} - E_{1,b}\|_{\Omega}^2 + \|\nabla E_{1,a} - \nabla E_{1,b}\|_{\Omega,t}^2 + \|E_{2,a} - E_{2,b}\|_{\Omega \times Y^2}^2 + \|\nabla_y E_{2,a} - \nabla E_{2,b}\|_{\Omega \times Y^2,t}^2 \leq 0.$$

Consequently,  $E_{1,a} = E_{1,b}$  and  $\nabla E_{1,a} = \nabla E_{1,b}$  almost everywhere on  $\Omega \times [0, t_m]$ ; similarly,  $E_{2,a} = E_{2,b}$  and  $\nabla E_{2,a} = \nabla E_{2,b}$  almost everywhere on  $\Omega \times Y^2 \times [0, t_m]$ .  $\square$

#### REFERENCES

- [1] G. ALLAIRE, *Homogenization and two-scale convergence*, SIAM J. Math. Anal., 23 (1992), pp. 1482–1518.
- [2] T. AMÉGLIO, F. W. EWERS, H. COCHARD, M. MARTIGNAC, M. VANDAME, C. BODET, AND P. CRUIZIAT, *Winter stem xylem pressure in walnut trees: Effects of carbohydrates, cooling and freezing*, Tree Physiol., 21 (2001), pp. 387–394.
- [3] A. BOSSAVIT AND A. DAMLAMIAN, *Homogenization of the Stefan problem and application to magnetic composite media*, IMA J. Appl. Math., 27 (1981), pp. 319–334.
- [4] J. E. BROWN, *Remaking maple: New method may revolutionize maple syrup industry*. University Communications, University of Vermont, Nov. 6, 2013. Available at <http://www.uvm.edu/~uvmpr/?Page=news&storyID=17209>.
- [5] M. CESERI AND J. M. STOCKIE, *A mathematical model of sap exudation in maple trees governed by ice melting, gas dissolution and osmosis*, SIAM J. Appl. Math., 73 (2013), pp. 649–676.
- [6] A. CHAVARRÍA-KRAUSER AND M. PTASHNYK, *Homogenization approach to water transport in plant tissues with periodic microstructures*, Math. Model. Nat. Phenom., 8 (2013), pp. 80–111.
- [7] D. CIRELLI, R. JAGELS, AND M. T. TYREE, *Towards an improved model of maple sap exudation: The location and role of osmotic barriers in sugar maple, butternut and white birch*, Tree Physiol., 28 (2008), pp. 1145–1155.
- [8] A. DAMLAMIAN, *How to homogenize a nonlinear diffusion equation: Stefan's problem*, SIAM J. Math. Anal., 12 (1981), pp. 306–313.
- [9] C. ECK, *Homogenization of a phase field model for binary mixtures*, Multiscale Model. Simul., 3 (2004), pp. 1–27.
- [10] D. GILBARG AND N. TRUDINGER, *Elliptic Partial Differential Equations of Second Order*, Springer, 2000.
- [11] I. GRAF AND M. A. PETER, *Homogenization of fast diffusion on surfaces with a two-step method and an application to T-cell signaling*, Nonlin. Anal. Real World Applic., 17 (2014), pp. 344–364.
- [12] I. GRAF, M. A. PETER, AND J. SNEYD, *Homogenization of a nonlinear multiscale model of calcium dynamics in biological cells*, Preprint des Instituts für Mathematik 2013–11, University of Augsburg, 2013. Submitted for publication.
- [13] U. HORNUNG, *Homogenization and Porous Media*, Springer, 1997.
- [14] R. W. JOHNSON, M. T. TYREE, AND M. A. DIXON, *A requirement for sucrose in xylem sap flow from dormant maple trees*, Plant Physiol., 84 (1987), pp. 495–500.
- [15] P. J. KRAMER AND J. S. BOYER, *The absorption of water and root and stem pressures*, in Water Relations of Plants and Soils, Academic Press, London, 1995, ch. 6, pp. 167–200.
- [16] J. L. LIONS AND E. MAGENES, *Non-Homogeneous Boundary Value Problems and Applications*, Springer, 1972.
- [17] M. MABROUK AND S. HASSAN, *Homogenization of a composite medium with a thermal barrier*, Math. Methods Appl. Sci., 27 (2004), pp. 405 – 425.
- [18] J. A. MILBURN AND J. KALLARACKAL, *Sap exudation*, in Physiology of Trees, A. S. Raghavendra, ed., John Wiley & Sons, New York, 1991, ch. 16, pp. 385–402.
- [19] J. A. MILBURN AND P. E. R. O'MALLEY, *Freeze-induced sap absorption in Acer pseudoplatanus: A possible mechanism*, Can. J. Bot., 62 (1984), pp. 2101–2106.
- [20] M. NEUSS-RADU, *Some extensions of two-scale convergence*, C. R. Acad. Sci. Paris, Ser. I, 322 (1996), pp. 899–904.
- [21] G. NGUETSENG, *A general convergence result for a functional related to the theory of homogenization*, SIAM J. Math. Anal., 20 (1989), pp. 608–629.
- [22] R. E. SHOWALTER, *Monotone Operators in Banach Space and Nonlinear Partial Differential Equations*, American Mathematical Society, 1997.
- [23] M. T. TYREE, *The mechanism of maple sap exudation*, in Tree Sap: Proceedings of the 1st International Symposium on Sap Utilization, M. Terazawa, C. A. McLeod, and Y. Tamai, eds., Bifuka, Japan, April 10-12, 1995, Hokkaido University Press, pp. 37–45.
- [24] A. VISINTIN, *Models of Phase Transition*, Springer-Verlag, 1996.
- [25] ———, *Homogenization of a doubly nonlinear Stefan-type problem*, SIAM J. Math. Anal., 39 (2007), pp. 987–1017.
- [26] T. R. WILMOT, *Root pressure in trees: A spring phenomenon*, Farming: Journal of Northeast Agriculture, (2011).

- [27] *Wood botany: Hardwoods and softwoods*. Workshop Companion. [http://workshopcompanion.com/KnowHow/Wood/Wood\\_Intro/Wood\\_Intro.htm](http://workshopcompanion.com/KnowHow/Wood/Wood_Intro/Wood_Intro.htm), accessed on October 30, 2014.